Pseudo-solid-state electrolytes utilizing the ionic liquid family for rechargeable batteries

AUTHOR(S):

Hwang, Jinkwang; Matsumoto, Kazuhiko; Chen, Chih-Yao; Hagiwara, Rika

ARTICLE

Pseudo-solid-state Electrolytes Utilizing the Ionic Liquid Family for Rechargeable Batteries

Received 00th January 20xx,
Accepted 00th January 20xx

DOI: 10.1039/x0xx00000x

Jinkwang Hwang,†*[a] Kazuhiko Matsumoto,†*[a] Chih-Yao Chen,†[b] and Rika Hagiwara[a]

The advent of solid-state electrolytes has unearthed a new paradigm of next-generation batteries endowed with improved electrochemical properties and exceptional safety. Amongst them, Li-stuffed garnet type oxides, sulfides, and NASICON type solid-state electrolytes have emerged with fascinating ionic conductivity, electrochemical stability, and high safety standards, besides creating an avenue for using metal anodes to maximize energy density. However, the actual performance of solid-state electrolytes is heavily encumbered by unexpected metal dendrite formation and typically manifests high resistances between the metal electrodes/solid-state electrolytes or grain boundaries, thereby restricting their practical applications. Recent studies have reported several novel approaches, such as modifying solid-state electrolytes using ionic liquids to form the so-called "pseudo-solid-state electrolytes". This class of electrolytes encompassing materials such as ionogel using ionic liquids and ionic plastic crystals has been gaining rekindled interest for their unique properties that promise great strides in battery performance and diversified utility. This minireview paper summarizes recent progress in pseudo-solid-state electrolytes utilizing ionic liquids, highlighting their fundamental properties while elaborating expedient design strategies. The realistic prospects and future challenges associated with developing pseudo-solid-state electrolyte materials present an insight into their properties to inspire far-reaching exploration into their material characteristics and functionalities.

Broader Context

Next-generation rechargeable batteries will have to demonstrate radical performance improvements based on; rate capability, cycleability, Coulombic efficiency, safety, and tolerance for wide temperature variations, to be worthy successors of Li-ion batteries. In a bid to satisfy these requirements, the development of novel electrolytes is quickly taking an important role in future battery systems expected to meet the insatiable demands for renewable energy, decentralized grids, and the momentous proliferation of electric vehicles. In this light, solid-state electrolytes have gained increasing recognition as the herald of a new paradigm of future batteries. However, the research attempts to implement these systems do not satisfy wide demands owing to the acute limitations associated with their electrolyte-electrode interface. As such, pseudo-solid-state electrolytes using ionic liquid (ILs), ionogels, and ionic plastic crystals (IPCs) have drawn attention to fill the shortcomings of the current organic solvent electrolytes and solid-state electrolytes from the unique properties of high thermal stability, good SEI formation, and high efficiency of lithium deposition and dissolution. These fascinating physical and chemical properties should improve the performance of secondary batteries. Besides their application in batteries, these energy materials are also considered ideal electrolytes for utility in capacitors and fuel cells. Indeed, pseudo-solid-state electrolytes are highly relevant to experimentalists and theoreticians in a range of different disciplines of inorganic chemistry, physical chemistry, polymer chemistry, electrochemistry, solid-state chemistry, materials science, physics, and simulation techniques. Through these materials, humanity makes another stride towards the next-generation rechargeable batteries.

1. Introduction

At the heart of modern technological marvels lies Li-ion batteries (LIBs), influencing innumerable innovations in portable electronics, electric and hybrid electric vehicles, and smart-grid systems.[1-3] The last two decades have seen massive evolutions in energy storage applications earmarked by progressive improvements in battery components, cells, and packaging culminating in the current commercial LIBs that utilize organic solvents alongside Li salts as electrolytes. Despite their success, there have been growing concerns over the encroaching LIB theoretical limits as societal demands continue to push the envelope of energy and power densities (fast-charging capability), lifespan, affordability, and safety in batteries. As such, there is a renewed urgency to pursue alternative chemistries such as Na, K, Al, Ca, Mg, and Zn for various frameworks such as ion, metal, sulfur, air, and solid-state electrolyte systems for next-generation batteries.[4-18]

Looking into the future, it is evident that electrolytes will continue to play a salient role in determining the performance

[a] Graduate School of Energy Science, Kyoto University, Yoshida, Sakyo-ku, Kyoto 606-8501, Japan.
[b] Precision Equipment Business Unit, KUBOTA Corporation, Osaka 581-8686, Japan.
*Correspondence and request for materials should be addressed to: KM (k-matsumoto@energy.kyoto-u.ac.jp) or JH (hwang.jinkwang.5c@kyoto-u.ac.jp
†Equal contribution.

parameters of batteries and the choice of components for a diverse range of applications. Until now, LIB contemporaries have relied on organic electrolyte systems, which employ mixtures of $LiPF_6$ and organic solvents, to achieve well-balanced electrochemical properties that support standard battery operations.[19,20] However, these electrolyte systems have poor tolerance for high-temperature variations, demonstrating poor conductivities at temperatures below 0 °C and decomposition at elevated temperatures above 60 °C. To address this issue, design trends for the next-generation batteries have shifted towards the solid-state class of electrolytes such as the Li-stuffed garnet $Li_7La_3Zr_2O_{12}$ (LLZO) and the sulfide solid electrolyte $Li_{10}GeP_2S_{12}$, which have exhibited remarkable ionic conductivities (0.3 mS cm^{-1} and 12 mS cm^{-1} at 25 °C, in their respective pure forms),[21,22] high thermal, chemical, and electrochemical stabilities as well as exceptional safety.[23-28] Besides their excellent electrochemical properties, solid-state electrolytes also facilitate the adoption of metal negative electrodes; envisaged as a prime negative electrode material for high energy density batteries. Moreover, the use of metal negative electrodes further unlocks the potential for developing other frameworks such as metal-sulfur and -oxygen batteries.[17,18,29-35] Although solid-state electrolytes used along with metal negative electrodes present excellent prospects for future batteries; their performance is heavily mired by severe dendrite formation and high interfacial resistance between the electrodes and the electrolyte during battery operations indeed a vexing problem for their practical utility. Typically, special fabrication techniques such as heating and pressing are employed to fill the gaps between the electrode and the electrolyte (solid-solid interface) caused by the highly reactive and uneven surface morphologies between the metal and solid-state electrolytes.[30,36-39]

Recent studies have reported several novel methods for modifying solid-state electrolytes using liquid phase additives to overcome their inherent limitations.[30,36-59] Among the numerous candidates for functional additives or conduction materials for solid-state electrolytes, ionic liquids (ILs) have drawn immense attention due to their unique set of properties that encompass: low flammability and vapour pressure, high electrochemical and chemical stabilities, and intrinsically high ionic conductivities.[60-81] These fascinating IL physiochemical properties not only renew the prospects of augmenting the safety and wide-temperature durability of the solid-state electrolytes but also promise to mitigate critical deficiencies such as poor contact relation and dendrite growth.[82-89] Moreover, the use of ILs also rekindles interest in other electrolyte frameworks such as ionic plastic crystals (IPCs) and ionogels, which constitute polymer electrolytes used alongside ILs. Consequently, a new class of electrolytes based on solid-state electrolytes and liquid electrolytes have been reported under various notations such as hybrid solid, solid like polymer, solid-liquid hybrid, dual-phase, quasi solid-state electrolytes, etc in the previous literature. These so-called "pseudo-solid-state electrolytes" not only augur great strides in battery performance and diversified utility but also present new prospects of addressing the prevailing issues in energy and secondary batteries. Here, the term “pseudo-solid-state electrolyte” is preferentially selected because it is not “solid-state” and can be mixed phases of liquid and solid phase or ionic plastic crystal phase. Comprehensive understanding of their properties and suggestion of future exploration into their material functionalities have served as the impetus for proposing this review topic. We focus on pseudo-solid-state electrolytes using ILs due to their vast range of possible applications in batteries for Li or metal batteries. Moreover, their physical and chemical advantages in the battery field are considered paths to new paradigms of future high-performance batteries. Besides their utilization as battery electrolytes, pseudo-solid-state electrolytes using ILs are also considered ideal for electrochemical capacitors and fuel cells applied in a wide range of disciplines.[90-95]

The present minireview aims to adumbrate the basic functionalities and characteristics of pseudo-solid-state electrolytes employing ILs by presenting their classifications and expounding on the fundamental physical and electrochemical properties that govern their performance in rechargeable batteries. We also cover potential applications in various battery systems. In the first part, the general properties of ILs are briefly summarised, followed by the effects of ILs on interfacial properties in rechargeable batteries. As Fig. 1 depicts, the pseudo-solid-state electrolytes utilizing ILs are classified into three categories: hybrid solid-state electrolytes, ionogels, and IPCs. In principle, the ILs in the pseudo-solid-state electrolytes serve as ion conductors that enhance the performance of the solid-state electrolytes. It should be noted that the distinct demarcation of the abovementioned categories is not straightforward because of unlimited combinations of components. Herein, we classified them based on the contribution to ion conduction in the pseudo-solid-state electrolyte for convenience of explanation. The second section introduces the concept of hybrid solid-state electrolytes. Here, solid-state electrolytes work as the primary ionic conductors, while the ILs are the subordinate ionic conductors. ILs are impregnated into the interfaces between electrode and electrolyte or solid electrolyte particles to enhance the interfacial phenomena at the electrode/electrolyte interface or grain boundaries.[30,36-57] For example, LLZO is the primary ion-conductor whereas IL covering LLZO particles is a subordinate ion-conductor but enhance interfacial properties. The third section then presents ionogels utilizing ILs,[96-110] wherein the ionogels have solid frameworks such as metal-organic frameworks, silica, TiO_2, and polymers impregnated with ILs. In this type of pseudo-solid-state electrolytes, ILs serve as the dominant ion conductors. The combination of various types of chemical frameworks and ILs presents a diverse platform for designing new electrolytes. Herein, polymer electrolytes, which constitute one of the most investigated fields in ionogels, are not covered because a number of excellent reviews have been published on polymer electrolytes using ILs.[111-118] The fourth section comprehensively reviews the IPCs because of their close resemblance to ILs.[119-130]

Studies have demonstrated the advantages of including IL domains in IPCs, renewing emphasis on their hallmarks as

pseudo-solid-state electrolytes. Fig. 2a shows a Ragone plot for various battery systems. Battery systems employing pseudo-solid-state electrolytes exhibit high specific energy with higher power densities than the current LIB systems because of their ability to perform at elevated temperatures. Moreover, the pseudo-solid-electrolytes are anticipated to have a high transference number of Li^+ and effectively higher ionic conductivities than liquid electrolytes, thereby providing fast-charge performance (Fig. 2b). Table 1 summarizes transport properties and the electrochemical test results of selected pseudo-solid-state electrolytes for secondary battery systems to give an overview of their present status. Detailed explanations of their properties and noteworthy achievements from previous explorations will be discussed in each section and further explicated by pertinent figures. The final section suggests design strategies for pseudo-solid-state electrolytes utilizing ILs to improve vital aspects such as safety, temperature range operability, and the performance of future batteries.

2. Ionic liquid Electrolytes

2.1 General features

Ionic liquids (ILs) encompass a class of liquids entirely consisted of cations and anions that can be combined to provide a wide variety of compounds.[62,64,66-81,131-142] This rich compositional flexibility presents a unique platform for designing new ILs, opening up infinite possibilities for new IL applications. In the search for next-generation batteries, ILs have gained immense attention as a potential replacement to conventional organic solvent electrolytes. Their exquisite properties such as low flammability, negligible vapour pressure, superior thermal and chemical stabilities, wide electrochemical window, and intrinsically fast ionic conductivity, foreshadow the development of safer batteries with broad operational temperature ranges.[134-146]

Out of the myriads of ILs developed so far, the selection of appropriate IL combinations for functional battery electrolytes is made by taking into consideration resultant physicochemical properties such as viscosity, conductivity, and melting points suitable for practical battery applications. Fig. 3 illustrates common cationic and anionic species used for ILs and ionic plastic crystals (IPCs) for electrolyte development. The choice of anions is relatively limited and typically entails fluorocomplex anions (PF_6^- and BF_4^-) and sulfonylamide anions, also denoted as sulfonylamides (TFSA$^-$ [TFSI$^-$] and FSA$^-$ [FSI$^-$]), as they have low melting points (wide liquid-state temperature range) and favourable conductivities compared to the conventional organic solvent electrolytes. Although PF_6-based organic solvent electrolytes are widely utilized in LIBs, they are not a common choice for ILs due to high viscosities and their vulnerability to hydrolysis. In contrast, ILs made from BF_4^- anions exhibit excellent chemical and electrochemical stability, although their time-consuming and expensive synthesis process is a major obstacle to their utilization.[143,144]

Accordingly, sulfonylamides have gained traction as the anion species of choice for IL electrolytes due to the hydrophobic nature of most sulfonylamide-based ILs that enables easy synthesis and facile purification.[5,85,87-89,145-157] Moreover, these ILs have high conductivities (i.e., 15.4 mS cm^{-1} for $[C_2C_1im][FSA]$[158]), and form robust, anion-dominant SEI layers that facilitate stable battery operations. In fact, recent studies have found FSA$^-$anions have a positive influence on the battery interfacial properties even when used in electrolytes that encompass ether-, carbonate-, or other IL-based anions.[159-164]

Still, in line with tuning the electrolyte properties, the melting point of ILs can be lowered to a certain extent by introducing bulky or long alky chains on the cations, although it comes at the cost of increased viscosity and decreased ionic conductivity, which has detrimental effects to electrochemical performance. In this context, the asymmetric organic cations of N_{nnnn}^+, P_{nnnn}^+, $C_nC_1pyrr^+$, and $C_nC_1im^+$ with alkyl chains have been used to formulate IL electrolytes with low melting temperatures. Although many ILs use organic cations, alkali metal cations such as Li^+, K^+, Rb^+, and Cs^+, can also provide ionic media. Inorganic ILs generally display higher melting points than that of their organic counterparts, making them suitable for elevated temperature operations. Furthermore, multiple inorganic salts can also be used to form inorganic salt mixtures to provide stabilization energy through the Gibbs energy of mixing, thereby decreasing the melting point to practical temperature ranges. For this reason, binary systems with M[FSA]-M'[FSA] and M[TFSA]-M'[TFSA] compositions and ternary systems in the form of M[FSA]-M'[FSA]-M"[FSA] and M[TFSA]-M'[TFSA]-M"[TFSA] (where, M, M', and M" = alkali metal cations) tend to demonstrate low eutectic temperatures (for example, Na[FSA]-K[FSA]-Cs[FSA] system demonstrates the lowest eutectic temperature of 36 °C[165]), making them prime candidates for ambient temperature applications. It should also be pointed out that these binary or ternary salt systems have also recently found utility in the formulation of superconcentrated electrolytes (salt in solvents, solvents in salt).[166-170] Inorganic salts can also be used alongside the series of glycol ethers (glymes) to formulate solvate ILs, which have recently become an attractive choice for battery electrolytes.[65,171-174] In this class of ILs, solvation is achieved when the lone pairs on the oxygen atoms in the oligo-ether act as a Lewis base to coordinate the Li (Na) cations (Lewis acids). For effective chelation, the amount of glyme mixed with the salt is regulated to allow complete coordination with the cations without leaving any free molecules. When used as battery electrolytes, solvate ILs have been found to facilitate the formation of robust SEIs with highly efficient Li or Na dissolution/deposition although temperatures should be closely monitored because glymes have lower thermal stability than inorganic or inorganic-organic ILs.

For a comprehensive coverage of IL electrolytes, it is important to mention protic ILs which are formed through a proton transfer between a Brønsted acid and a base. Although these ILs have simple and inexpensive synthetic processes compared to aprotic ILs, they are not widely used in secondary batteries due to safety concerns related to hydrogen evolution. However, it is worth mentioning that protic ILs based on [TFSA]$^-$

and [FSA]$^-$ have shown high electrochemical stability and excellent physiochemical properties in some cases.[175,176]

Additional physicochemical characteristics of ILs will be presented in a later section in comparison to the basic characteristics of IPCs (Section 5). For detailed explanations of the thermal, physicochemical, and electrochemical properties, as well as the basic experimental know-how for handling ILs, it would be recommended to refer to previous reviews and literature that adequately cover the subject matter in detail.[5,177] Although there are many noteworthy properties, applications and milestones achieved by ILs so far, this minireview shall not cover the entirety of such research and achievements for concision, and thus other literature would be recommended for such scope.[132,178-182]

2.2 Effects on interfacial behaviour of rechargeable batteries

In the race towards next-generation batteries, Li metal has been envisioned as the ultimate negative electrode material due to its extremely high theoretical specific capacity (3860 mA h g^{-1} in the charged state) and its potential to dramatically improve the energy density of future batteries. Unlike the conventional graphite negative electrodes which operate through Li (de)intercalation reactions during charge-discharge, the lithium metal batteries function through a series of Li metal deposition and dissolution which leads to the invariable formation of Li dendrites a critical impediment to efficient operations. This Li dendrite formation, which is so far the biggest limitation to the implementation of this battery technology, creates severe problems such as; (i) shortened battery lifespan caused by the chemical exhaustion of the Li metal electrode and the electrolyte, (ii) diminished battery performance during operations, (iii) safety issues resulting from internal short-circuiting, and (iv) the accumulation of dead Li layer(s) that would hinder Li diffusion, reducing the energy efficiency.[82-89] As such, extensive studies have been commissioned in search of a viable interface between Li metal and electrolytes that would herald the age of practical Li metal batteries. Consequently, this pursuit has also given rise to the new field of research on pseudo-solid-sate electrolytes as another avenue for improving battery performance.

Several studies entailing symmetric metal deposition/dissolution tests using IL electrolytes have reported superior cyclability, high coulombic efficiency, smaller overpotential, and suppressed dendrite formation in comparison to conventional organic solvent electrolytes. These electrochemical capabilities can largely be attributed to their high thermal and chemical stability in addition to their remarkable metal dendrite suppression capabilities that enable them to form robust solid-electrolyte interphase (SEI) layers on negative electrodes.[86,183-186] As such, ILs would be uniquely positioned to enhance the electrochemical performance of solid-state electrolytes.

For better insight, Fig. 4a shows surface SEM images of Li metal pre-treated with [C_3C_1pyrr][FSA] ILs comprising Li[FSA] (Fig. 4a(a)-(d)), Li[PF_6] (Fig. 4a(e)-(h)) and Li[AsF_6] (Fig.4a(i)-(l)) Li salts, respectively.[183] As shown in the images, the surface morphology of Li metal changes, depending on the treatment duration and the Li salt species used. Further, XPS analysis confirmed that the SEI components consisted of LiF, Li_2CO_3, $LiSO_2F$ derived from the anion species while the species derived from the cations were affirmed through Hofmann elimination. Additionally, the SEI layer formed by the ILs (12 days pre-treatment) achieved improved cyclability by suppressing the dendrite formation and mitigating electrolyte degradation. However, the Li metal electrode pre-treated for 18 days exhibited unstable cycle performance, indicating the dense and rough SEI formed over a longer pre-treatment duration was not effective in enhancing the electrochemical performance.[183]

In another study (Fig. 4b), the dendrite suppressing capabilities of ILs and organic solvent electrolytes were investigated through Li dissolution/deposition tests carried out using two Li metal electrodes inserted in 30 mol% Li[FSA]-[C_2C_1im][FSA] IL electrolyte and 1 mol dm^{-3} Li[PF_6]-EC-DMC (1:1 vol/vol) organic solvent electrolyte at 8.0 mA cm^{-2} for 210 min (8 min per cycle) in glass beaker cells at ambient temperatures.[187] Optical measurement confirmed the stark contrast between the Li deposition/dissolution behaviour in the IL and organic solvent electrolytes, as shown in the illustration (Fig. 4b). In the organic solvent electrolyte, severe dendrite growth commenced in the initial stages of the cycle test, followed by a vigorous accumulation of dead Li layers and a significant increase in the cell's overpotential, which eventually resulted in a short circuit. In contrast, the IL electrolyte cell displayed a uniform Li metal deposition with minimal accumulation of the dead Li layers, along with a stable cycle maintained until the end of the measurement. These observations confirm the formation of an SEI layer with excellent dendrite suppressing properties in IL electrolytes, in conformity with other previously reported works.

3. Hybrid solid-state electrolytes with ionic liquids

This section will provide a brief highlight on the preparation and fabrication methods of hybrid solid-state electrolytes using IL electrolytes and explicate their improved performance. We further discuss the prospects of finding new physicochemical and electrochemical properties in pseudo-solid-state electrolytes with the aim of advancing their progress. Table 1 summarizes selected examples of hybrid solid-state electrolytes using ILs and IPCs.

3.1 Interfacial properties

Pseudo-solid-state electrolytes comprising hybrid IL solid-state electrolytes are prepared by encapsulating solid-state electrolytes in ILs to create a hybrid mixture of two ion conductors as illustrated in Fig. 5.[30,36-57] In this approach, solid-state electrolytes are used as the main ion conductors while ILs act as subsidiary ion conductors, unlike the ionogel pseudo-solid-state electrolytes which will be covered in detail in the next section (Section 4). Besides their role as ion conductors, ILs also play the critical role of interfacial wetting by modifying the electrode/solid-state electrolyte or solid-state electrolyte/solid-state electrolyte (grain boundary) interfaces. Even so, it should be noted that even when incorporated into solid-state

electrolytes, the ILs retain their intrinsically high electrochemical stability. In fact, the limit potentials of the hybrid IL solid-state systems are typically determined by the constituent ILs. Further, the robust SEI layers protecting the solid-state electrolyte and electrode are mainly products of IL decomposition.

In one preparation method, a simple interfacial modification was done by adding small amounts of 20 mol% Li[TFSA]-[C_4C_1pyrr][FSA] IL to the interface between $LiFePO_4$/LLZO, as shown in Fig. 5a. Subsequently, EIS measurements were conducted on symmetric Li/LLZO/Li cells with and without the IL to compare their interfacial resistance. In the cell without the IL, a large interfacial resistance of 4900 Ω cm^2 was observed, whereas the cell with the 20 mol% Li[TFSA]-[C_4C_1pyrr][FSA] IL demonstrated remarkable improvements in the interfacial properties which were embodied by the significantly reduced interfacial resistance of 290 Ω cm^2. Further, Li deposition/dissolution tests also pointed out that the addition of the IL lowered the overpotential and improved cyclability, achieving higher efficiencies as well as favourable dendrite suppression.[38] In another preparation method, a hybrid solid-state electrolyte was prepared by gentle ball-milling a mixture of LLZO solid-state electrolyte and 5 mol% Li[TFSA]-[C_4C_1pyrr][TFSA] IL at 40 rpm for 1 h under Ar (25 °C). As shown in the SEM images of the resultant material in Fig. 5b, the LLZO particles are sufficiently covered by the IL.[39] The ball-milled mixture of LLZO and IL further demonstrated an ionic conductivity of 0.4 mS cm^{-1}, suppressed dendrite formation, high capacity retention of 99% after 150 cycles in the Li/$LFePO_4$ cell and a high thermal stability up to 400 °C.[39]

It is worth noting here that organic solvent electrolytes and conventional organic additives can also be used to improve the interfacial wetting and thereby reduce the interfacial resistance of the solid-state electrolytes. However, safety concerns related to their high flammability and volatility makes them unfavourable for treating solid-state electrolytes. Conversely, IL electrolytes exhibit high thermal stability even with solid-state electrolytes making them prime candidates for a variety of practical batteries. In fact, for comparison, a sulfur electrode taken from [AC_1im][TFSA] IL and another from 1 mol dm^{-3} Li[TFSA]-DME:DOL (1:1 v/v) organic solvent electrolyte, were subjected to flammability tests as illustrated in Fig. 5c. As expected, the electrode with the organic solvent electrolyte promptly ignited whereas no flame was observed in the case of the electrode covered in the IL. These studies clearly demonstrate that the IL ameliorates the contact between the Li metal electrode and solid-state electrolyte effectively enhancing their electrochemical performance without compromising safety.[57]

Efforts to realize safe battery operations have also prompted further exploration into hybrid IL solid-state electrolytes prepared using glyme-based solvate ILs which are known to have low flammability. Several studies have reported improved electrochemical performance in hybrid solid-state electrolytes prepared using solvate ILs made from tetraglyme (G4) or triglyme (G3) and Li[TFSA] salt alongside solid-state electrolytes (Fig. 5d).[41,42,44,48,53,54] In a report on a pseudo-solid-state electrolyte using a sulfide solid-state electrolyte Li_3PS_4 and solvate IL Li[TFSA]-G3, the ionic contact between the electrolyte and the Li metal electrode was found to significantly improve upon the addition of the solvate IL. In fact, the charge-discharge of $LiFePO_4$/Li cell comprising the solid-state electrolyte alone was not possible and could only be conducted upon the addition of Li[TFSA]-G3 IL. The poor performance of the solid-state electrolyte is attributed to deficiencies in the solid-solid contact (voids between solid electrolyte and active material) that hinder the facile diffusion of Li^+. However, Li[TFSA]-G3 IL fills the voids in the solid-solid interface with high efficacy, resulting in improvements in electrochemical performance.[56] Besides optimizing solid-state electrolyte performance, glyme-based solvate ILs have also been utilized in the fabrication of flexible pseudo-solid-state electrolytes prepared using a solid-state electrolyte, a solvate IL, and a polymer.[41] In a recent study, an Al-doped LLZO, Li[FSA]-G4 IL, and polystyrene (PS) were ball-mixed in toluene and the resulting slurry was cast on poly(ethylene terephthalate) and dried under vacuum. The resulting electrolyte was not only flexible, but also had a high ionic conductivity of 0.1 mS cm^{-1}. By the same token, UV-cross-linked polymers have recently emerged as attractive casting materials for solid-state electrolyte and liquid mediums.[58,59] For instance, a recent study on a hybrid solid-state electrolyte utilising a benzophenone UV initiator alongside LLZO and Li[TFSA]-G4 reported the system to have high thermal and electrochemical properties.[58]

3.2 Applications in Lithium and sodium secondary batteries

Sulfides such as $Li_{10}SnP_2S_{12}$ (LSPS) have also emerged as promising solid-state electrolyte candidates on account of their exceptionally high ionic conductivities (14 mS cm^{-1} for $Li_{10}SnP_2S_{12}$) that even supersede those of some conventional organic solvent electrolytes. However, their electrochemical performance is immensely inhibited by high interfacial resistance between the electrode and the electrolyte. Furthermore, LSPS is highly reactive particularly when in contact with Li metal. Even at a low potential, Li metal causes spontaneous electrolyte decomposition resulting into the formation of a highly resistive interface comprised of Li_2S, Li_3P, and Li-M alloys. The resultant alloy species, specifically Li_3P, and Li-M, tend to be ineffective in preventing further electrolyte decomposition and therefore allows further deterioration to continue.[188]

In a study on a hybrid solid-state system, cyclic performance tests were conducted on a symmetric Li/LSPS/Li cell containing 1.5 mol dm^{-3} Li[TFSA]-[C_3C_1pyrr][TFSA] IL and another without the IL to ascertain the effects of the IL on the electrolyte/electrode interfacial properties. In absence of the IL, the overpotential of the cell is found to dramatically increase with progressive cycling, an indication of continuous decomposition of LSPS caused by the reaction with Li metal (Fig. 6a). On the other hand, the cell containing 1.5 mol dm^{-3} Li[TFSA]-[C_3C_1pyrr][TFSA] IL exhibited stable cycle performance without an increase in overpotential for over 1000 h (Fig. 6a). As shown in Fig. 6b, the addition of IL into the sulfide solid-state electrolyte also reduced the interfacial resistance of the Li/Li

symmetric cells from 1960 to 250 Ω that similar to the observation in the hybrid LLZO system mentioned in a previous section. Furthermore, charge-discharge profiles (Fig. 6c) obtained from Li/$LiFePO_4$ cells demonstrated that the addition of the IL led to improved electrochemical performance characterized by reduced polarization and large reversible capacities. These observations further indicate that the IL improves the interfacial behaviour by enhancing the wettability between the Li metal and the rough and uneven surface of the solid electrolyte to provide better cycle performance as seen in Fig. 6d.

The use of ILs to enhance the performance of solid-state electrolytes is by no means limited to Li systems. In a previous report, [C_3C_1pyrr][FSA] IL and 0.8 mol dm^{-3} $Na[PF]_6$-EC-DMC organic electrolyte were added to the NASICON-type $Na_3Zr_2Si_2PO_{12}$ solid-state electrolyte to fabricate two-hybrid solid-state electrolytes for Na secondary batteries. Subsequent electrochemical performance tests were conducted on cells comprising $Na_3V_2(PO_4)_3$ positive electrode, Na metal negative electrode and the two-hybrid solid-state electrolytes alongside an untreated solid-state electrolyte. Charge-discharge tests conducted on a cell with the untreated solid-state electrolyte yielded a limited capacity of 85 mAh g^{-1} in the first cycle and showed poor cyclability at room temperature. On the other hand, the addition of a small amount of [C_3C_1pyrr][FSA] IL resulted in improvements in the rate performance (86 mAh g^{-1} at 10 C at room temperature) and the cyclability (90 mA h g^{-1} after 10,000 cycles at 10 C with the high average coulombic efficiency of ~100.0%) of the cell (Fig. 6f). These EIS results affirmed that even in Na systems, the introduction of an IL into the electrolyte system helps reduce the total resistance.

In a control experiment, when 0.8 mol dm^{-3} $Na[PF]_6$-EC-DMC organic solvent electrolyte was added to the solid-state electrolyte instead of the IL, the interfacial resistance decreases to tens of ohms, in a similar manner as the IL (Fig. 6e). However, the discharge capacity faded away after 250 cycles due to electrolyte decomposition, indicating that the IL facilitated better electrochemical performance in the solid-state electrolyte compared to the organic electrolyte, by providing better contact relation between the solid-solid particles thus forming ion migration paths between the active material and solid-state electrolyte.

The simplicity in the preparation of hybrid IL solid-state electrolyte systems makes them a feasible and accessible route for enhancing the performance of solid-state electrolytes. Through this approach, it is possible to capitalize on the advantages of solid-state electrolytes, such as their safety, while mitigating their high interfacial resistance. Moreover, the exceptional capabilities to form stable and robust SEI layers render ILs as exemplary materials for alleviating electrolyte decomposition and suppress dendrite formation. However, this class of pseudo-solid-state electrolytes is still in its incipient stages. For instance, the influence of the liquid to solid component ratios and the porosity of constituent solid compounds on the electrochemical and mechanical properties of the hybrid IL solid-state electrolytes is not well understood. Nonetheless, the chemical diversity of ILs provides nearly infinite electrolyte compositions that hold promise for future battery systems. Still, it should be noted that exploring these infinite combinations and parameters calls for rigorous efforts and time which may delay the progress of these materials.

4.Ionogels

Ionogels are categorized as one of the typical types of pseudo-solid-state electrolytes that fully utilize the unique features of ILs. They have a broad range of applications owing to their simple structural modes and facile synthetic routes. This section describes the general features and applications of ionogels in Li metal batteries of ionogels.

4.1 General features of ionogels

Ionogels (also referred to as ion gels) constitute a class of stable solid-liquid hybrid systems, in which a continuous solid network spans throughout a liquid phase (in this case an IL), as shown in Fig. 7.[97,189-192] First reported in 2000, this class of IL-based hybrid materials has been gaining increasing recognition for its fascinating combination of exquisite chemistries and intrinsic functionalities begotten from an IL hosted within a mesoporous solid matrix.[107,110,193-196] In their utility as pseudo-solid-state electrolytes for rechargeable batteries, ionogels engender manifold prospects and advantages over pure ILs such as: (i) improved transport properties springing from the enhanced dissociation of charge carrier ions and/or the anchoring of anions, which could potentially contribute to higher rate capabilities (Fig. 8),[147,197-201] (ii) a wider usable temperature range resulting from retarded glass/freezing transition or thermal decomposition,[199,202-207] (iii) solid-like characteristics such as leak-proof and mechanical robustness,[105,207] (iv) and other complementary functionalities such as the regulation of the deposition behaviour of metallic anodes[109,208-212] to eliminate the crossover of undesirable species, *et cetera*.[209,210] From a practical viewpoint, formulating a suitable ionogel composition has the potential to improve their processing compatibility and portability, reduce the quantity of ILs required for a certain scale of applications,[101] and eliminate the need for separators, thus enabling simplified and cost-effective battery assembly.[108,204] Moreover, the ILs within some ionogels can easily be recycled by disassociating the solid phase using miscible solvents, making them sustainable options as battery components. [213] Based on the nature of the solid matrix, ionogels can be categorized into polymeric, inorganic, and hybrid organic-inorganic materials.[101,191] It is imperative we point out that recent developments in polymer-based electrolytes with ILs for energy-related applications, either through the polymerization of ILs or through the dispersion of ILs in solid polymers, has been comprehensively summarized by a number of authoritative groups.[111-118] Therefore, for the succinctness of this minireview, interested readers would be advised to look into these reviews. Also, it should be noted that in reference to this electrolyte system, several arbitrary terms such as poly(ionic liquid)s, gel polymer electrolyte, solid (hybrid) polymer electrolyte, plasticized electrolyte, and rubbery

electrolyte have been used, and thus reader discretion is advised.[112]

In regards to inorganic solid matrices, their interaction with ILs and the confinement effect have been known to play a crucial role in endowing ionogels with unmatched properties.[97,191,192] In particular, confining ILs into minuscule spaces, where at least one dimension is comparable to the size of the constituent ion(s), not only creates a different microenvironment for the IL (compared to the bulk phase) but also promotes a strong interaction between the ILs and the matrix surface, resulting in different structures, dynamics, phase transition behaviour *et cetera*.[214] Thus, nanoporous materials such as (ordered) silica (SiO_2),[96,100,102,106,197,204,205,215-220] alumina (Al_2O_3),[221,222] zirconia (ZrO_2),[223,224] titanium dioxide (TiO_2),[200,206,225] boron nitride (BN),[199,207] and metal-organic frameworks (MOFs)[199,202,209,226,227] have been exploited for the design of ionogels (Table 1). Apropos the synthetic strategy of ionogels, given that the filling process is usually carried out under reduced pressure, the lack of appreciable vapour pressure for ILs makes it more feasible to prepare a veritably confined liquid in comparison to other molecular solvent-based electrolytes.[101]

For the systems shown in Figs. 8 and 9, the ionic conductivities of the ionogels are >1.0 and 0.3 mS cm^{-1}, respectively (summarized in Table 1); Thus, the ionic conductivity is seen to decrease by approximately one order of magnitude when ionogels are formed. Despite the decrease in ionic conductivity, the cells using ionogel electrolytes can still deliver better performance under certain conditions. This shows that a high bulk ionic conductivity is not necessarily a prerequisite for achieving decent electrochemical performance (provided that a minimum conductivity is maintained).

4.2 Applications in lithium metal batteries

The development of ionogels as pseudo-solid-state electrolytes for rechargeable lithium batteries has been a burgeoning area of interest. In a recent study, an ionogel that consolidates liquid-like ion conductivity and solid-like modulus was demonstrated by Hersam and co-workers.[207] In their work, hexagonal boron nitride (hBN), a structural analogue of graphene, was adopted as the host matrix on account of its appealing attributes, which include: chemical inertness, electrical insulation, thermal stability, as well as excellent mechanical properties. In order to accelerate the IL adsorption and maximize the resultant mechanical strength; a few-layer-thick and size-controlled hBN nanoplatelets (143 ± 67 and 2.4 ± 1.2 nm in lateral dimension and thickness, respectively) were prepared through an efficient liquid-phase exfoliation method with the aid of a stabilizing polymer, ethyl cellulose (EC) (Fig. 8a).[207] The hBN/EC mixture was then subjected to annealing at 400 °C in the air to decompose the EC, creating a thin carbon coating on the surface of hBN (Fig. 8b, c). Thereafter, the ionogel was prepared by physically mixing the exfoliated hBN nanoplatelets with excess Li[TFSA]–[C_2C_1im][TFSA] IL and aged at ambient temperatures. Viscoelastic measurement(s) and visual confirmation were subsequently carried out to confirm the mechanical properties of the resulting product (Fig. 8d). IL-based ionogels draw in the benefits of extremely low vapour pressure and antistatic properties from the constituent ILs, allowing them to withstand the high-vacuum conditions necessary for electron microscope characterization,[228] which in this case, showed the exfoliated hBN nanoplatelets to be completely covered by the IL (Fig. 8e). Even more importantly, this ionogel electrolyte was found to have a shear storage modulus as high as 5 MPa and a sufficient room-temperature ionic conductivity for electrochemical applications (> 1 mS cm^{-1}), superseding most IL-based ionogel electrolytes made from common inorganic hosts such as SiO_2[208] or other previously reported polymers.[229] These advantages are attributed to two factors: (i) the carbon coating enhances the interparticle interactions among the hBN nanoplatelets and (ii) the nanoscale size of exfoliated hBN reinforces gelation without disrupting ionically conductive pathways in the electrolyte. To evaluate the electrochemical performance of this material, a test cell with a binder-free and thermally stable $LiFePO_4$ positive, a Li metal negative electrode, and the ionogel electrolyte were assembled without a separator. As shown in Fig. 8f, a discharge capacity of 150 mAh g^{-1} is achieved at room temperature, but the full potential of the Li/$LiFePO_4$ cell is unleashed during elevated temperature operations at 175 °C where remarkable rate capabilities and excellent reversible capacities were attained (see Fig. 8g for cycle performance at 10C).[230]

Metal-organic frameworks (MOFs), also known as porous coordination polymers (PCPs), are another evolving class of crystalline materials built by connecting metal nodes with organic linkers, to form cavities and channels akin to those in zeolites.[231] These materials have highly tailorable compositions, framework topologies, surface areas, and porosities which help manipulate their interactions with guest species; making them promising components for hybrid materials, in particular, ionogels.[232-236] This type of material was first studied and reported in 2015 by Kitagawa and co-workers who incorporated Li[TFSA]–[C_2C_1im][TFSA] IL into the micropores of ZIF-8 through physical mixing and subsequent heating to prepare an ionogel with no glass transition or freezing unlike the bulk IL which freezes upon cooling.[202] This difference in phase behaviour was attributed to the presence of $[TFSA]^-$, which is unable to construct crystal or glass structures with $[C_2C_1im]^+$ and Li^+ in the micropores due to its relatively large van der Waals volume (147 $Å^3$)[237] in comparison to the inner volume of each micropore of ZIF-8 (817 $Å^3$). On an interesting note, even though the self-diffusion coefficient of Li^+ in the ionogel was significantly lower than that of the bulk IL, the activation energy required for the self-diffusion of Li^+ was still comparable to that of the bulk IL (15.7 and 18.6 kJ mol^{-1}, respectively). This implies that Li^+ conduction in ionogels is not interrupted by the host framework and involves an exchange with the solvating $[TFSA]^-$. In another recent study, an ionogel was fabricated using MOF-525(Cu) and Li[TFSA]–[C_2C_1im][TFSA] IL, as illustrated in Fig. 9a.[199] Here, the aperture size of the MOF (12 × 7 Å) was slightly greater than that of $[TFSA]^-$ (7.9 × 2.9 Å) and $[C_2C_1im]^+$ (7.6 × 4.3 Å),[238] imposing a steric restriction on the ions unrelated to the reaction, and thus improving the transference number of Li ions (from 0.14 to 0.36). Furthermore, the 3D open channels within the MOF are posited to engender numerous direct-contact

points between the electrode materials and the confined Li^+ cations, resulting in numerous "nanowetted" interfaces that facilitate favourable electrochemical reactions. With such an interface in place, the local Li^+ flux near the electrode is expected to be homogenized, effectively addressing the Li dendrite issue that afflicts the practicality of conventional solid-state electrolytes.[239] As shown in Fig. 9b, the Li/Li symmetric cell using the ionogel electrolyte exhibits a stable cyclability with a small deposition-dissolution overpotential of 40 and 70 mV at current densities of 0.05 and 0.2 mA cm^{-2}, respectively. In comparison, the typical overpotential observed in solid-state electrolytes falls in the range of several hundred mV under similar cycling conditions.[31] Besides, this ionogel electrolyte, when used in Li/$LiFePO_4$ cell (Fig. 9c), demonstrated stable operations over a wide temperature range (–20 to 150 °C) conditions hardly tolerable for conventional solid-state electrolytes. This not only affirms the feasibility of ionogels as electrolytes but also offers the prospects of expanding the application frontiers of secondary batteries.

Leveraging the vast chemical space occupied by ILs and the numerous nanoporous solid hosts in existence, ionogels open a whole new dimension of systematic modulation of electrolyte characteristics for a vast array of applications. In a broad sense, ionogels represent a limitless canvas for chemists to showcase their aptitude by creating novel materials with unparalleled capabilities through simple, logical extrapolations. Also, in place of ILs, metal salts can also be incorporated into certain solid hosts to create single-ion conductors (e.g., Na, Mg, and Al); an avenue that also brings a lot of prospects to the future of batteries.[240,241] Hew phases which may negatively influence the electrode kinetics.[242] In addition, the correlation between the electrolyte volume and the total pore volume of the other cell components could be an area of concern because the possibility of a “dead volume” formed by the solid host could be detrimental to electrochemical performance.

5. Ionic plastic crystals

Ionic plastic crystals (IPCs) are a class of crystalline materials that facilitate solid-state ion conduction either through their constituent ions or via doping. As shown in Fig. 10, IPCs are known to exhibit an assortment of structural configurations that are inextricably connected to variations in temperature. Although IPCs themselves are pure solid-state electrolytes, they share many characteristics with pseudo-solid-state electrolytes fabricated using ILs. In fact, in recent works, many IPCs containing metal ions have been found to behave like pseudo-solid-state electrolytes, drawing interest in their use as battery components. Thus, in this section, we extensively review IPC features, mechanisms, and their performance as electrolytes in secondary batteries.

5.1 General features of ionic plastic crystals

Currently observed plastic crystals are generally characterized by a long-range ordering with local orientational disordering of constituent species falling within two distinct phases, namely the highly ordered crystals and isotropic liquids.[243,244] The highly disordered structures of plastic crystals are marked by a low entropy change during melting (20 J mol^{-1} was proposed for molecular plastic crystals), engendering a rotating motion of the constituent ions which increases the ionic conductivity even at room temperature. [243] This rise in ionic conductivity as a result of the rotating motion of ions is not exclusive to IPCs. Inorganic compounds such as Li_2SO_4 have similar mechanisms for ionic conductivity, although high temperatures are needed to induce the rotating motion.[245] The application of IPCs as electrolytes for secondary batteries has been investigated from various perspectives.[121,130,177,246,247] However, in this section, we focus on the IPCs observed at room temperature, which are regarded as a close family of ILs and shares similar ionic species (mostly organic cations and thus often called organic ionic plastic crystals (OIPC)).

Ionic species, such as those summarized in Fig. 3 (also used for IL formulation) as well as relatively spherical ions (aliphatic alkyl-ammonium and phosphonium sometimes with ring structures) are usually preferred for the fabrication of IPCs, although aromatic cation-based salts such as alkylimidazolium cations can also be used due to their similarities in plastic behaviour and related dynamics of molecules.[248,249] Alkylpyrrolidinium cations with a nitrogen-containing five-membered ring represent an eminent family of cations known to exhibit a manifold of fascinating ion motions with temperature variations;[250-252] For instance, low temperatures engender temperature-induced puckering and liberational motions of the ring along with the rotational motion of side-chains, whereas high temperatures exhibit shifts in the rotation of the entire cation (either uniaxial or isotropic).[253] These unique correlations between ionic motions and temperature make this family of cations ideal for the formulation of a variety of IPCs suitable for wide-ranged temperature operations. A schematic illustrating the structural information and appearance of IPCs is furnished in Fig. 11. Similar to ILs, IPCs are characterized by negligible volatility and flammability and thus present great advantages in terms of the safety of secondary batteries.[130] Furthermore, the plasticity of IPCs and related mechanical properties, which lack in most inorganic solid-state ion conductors, offers additional advantages such as improved contact between electrolyte and electrodes,[254] as illustrated by the flexible self-standing film in Fig. 11a[255] (mixing of IPCs with polymer or polymeric ILs also results in the flexible film (Fig. 11b[127])).

In most cases, organic salts possessing an IPC phase, melt into an IL phase via several solid-solid transitions during heating. Here, the ionic motion is seen to increase as the material undergoes each transition.[253,256-275] Structural studies on alkylammonium salts with highly symmetrical anions revealed simple crystal structures characterised by high symmetries (sometimes cubic phases such as NaCl-and CsCl-type) in the highest temperature phase as a result of the (pseudo-)rotation of the constituent ions.[276-279] The TFSA anion, which is a typical IPC forming ion, undergoes some disordering modes similar to those confirmed in organic cation compounds.[258,280-282] The standard disordering mechanisms in the solid-state entail the presence of two trans $TFSA^-$ conformers akin to those observed

in previous crystallographic works on $[C_2C_1pyrr][TFSA]$[258] and $[N_{2222}][TFSA]$[256] (Fig. 11c). Analysis of $[P_{122i4}][PF_6]$ by a combination of several analytical methods (XRD, NMR, DSC, ionic conductivity, and SEM) further affirmed that the ionic motion of IPC forming salts typically depended on temperatures.[283] At the low-temperature phase, the methyl and ethyl groups of P_{122i4}^+ gradually begin to rotate, eventually causing the anion to tumble isotropically (Fig. 11d). However, when the temperature is raised, the cation first uniaxially rotates and then isotropically tumbles, resulting in anion diffusion. Both the cations and the anions can diffuse in the highest temperature phase where a small residual entropy of 5 J K^{-1} mol^{-1} is needed for melting. These evolutions in molecular motion have been adequately confirmed through molecular dynamics simulations.[284]

Besides their unique ionic mobility, IPC electrolytes are also endowed with fascinating mechanical properties such as plasticity which improves the electrolyte-electrode contact. Even so, quantitative analysis studies on their mechanical properties are very limited.[244] In the case of molecular plastic crystals, the correlation between their structures and mechanical properties have been well-explicated by studies on their molecular symmetries and intermolecular interactions.[285,286] However, such insights on IPCs remain scarce, calling for more scientific rigour into their explorations. In a bid to exploit this niche, a mechanical analysis employing a static force of 1.7 N on $[C_3C_1pyrr][PF_6]$ IPC found the mechanical properties to be highly phase-dependent. The phase transitions induced by temperature elevations resulted in enhanced plasticity, ascribed to the increase in vacancies.[260] Due to the highly deformable nature of IPCs at high temperatures, polymer materials are typically added to provide mechanical support during operations (see Section 5.5).[128,260,287,288]

5.2 Ionic conductivity

In general, the ionic conductivity of the IPC-forming salts is characterized by slight (or in some cases significant) increases via step-like progressions at each solid-solid transition due to enhanced ion motion caused by increasing temperatures.[257,259-264,266-269,271-274] This behaviour is contrary to the observations from NMR and XRD measurements conducted on $[C_1C_1pyrr][BF_4]$[289] and [TEMMP][TFSA][290]; where ionic conductivities were noted to drop at the solid-solid transition from low to high temperatures. Predictably, IPC ion conduction mechanisms depend on the type of conducting species as well as the rotational, translational, and conformational disorders (Fig. 11e).[291] However, defects such as vacancies are also posited to contribute to ion conduction, as has been confirmed through positron annihilation lifetime spectroscopy which revealed that both the vacancy size and connectivity influence ion conduction in plastic crystals.[274,275,292,293] Further, the role of vacancies has also been explored through molecular dynamics simulations pertaining dynamic heterogeneity.[283,294] In this context, the heterogeneous dynamics in different phases observed through magnetic resonance imaging alongside other spectroscopic measurements not only suggested the presence of both dynamic (IL-like) and static domains within the OIPCs but also attested the dependence of ion transport on crystallization conditions.[125,135,295,296] Other important factors that determine the dynamic behaviour of IPCs include ionic (ion-ion) correlation, which has recently been reported to play a critical role in ionic conductivity in place of ion diffusion (Fig. 11e). The report further demonstrated that ionic (ion-ion) correlation in some cases even suppresses ionic conductivity to 100 times lower than the estimated diffusion coefficients derived from the Nernst-Einstein equation.[297] In the same vein, studies on alkylpyrrolidinium IPCs with various anions revealed a correlation between the ionic conductivity and the radius ratio; whereby smaller radius ratios resulted in high ionic conductivities.[266,267]. Likewise, chirality which affects the structural properties of organic salts, was also noted to be a contributing factor to the dynamic behaviour of IPCs.[298,299]

High ionic conductivity is a key prerequisite for the functionality of any electrolyte material, making the efforts to enhance ionic conductivity in IPCs a critical aspect of their advancement. Doping of metal ions such as Li^+ to IPCs has been found to be an expedient way to raise ionic conductivity.[124,126,275,300-305] For instance, doping $[C_2C_1pyrr][TFSA]$ with 1 mol% Li[TFSA] was found to result in a 20-fold increase in conductivity at 25 °C. The enhanced Li^+ diffusion in the IPC phase has been attributed to the formation of a solid-solution phase between the IPC frame and the Li salt, leading to the formation of a defect.[306]

An alternative conduction mechanism for Li-ions was also proposed based on the existence of the IL phase in an IPC lattice. Here, the conduction pathways appeared disconnected, forming droplets at low concentrations. However, at high concentrations, the conduction pathways became convoluted and interconnected.[307] The minimum energy path of Li-ion diffusion calculated from theoretical simulations on the $Li[PF_6]$-$[C_3C_1pip][PF_6]$ IPC indicated that the Li-ion moves in concert with PF_6 octahedral rotation, changing its coordination numbers between two and three.[308] Further, a molecular simulation study on the $[P_{122i4}][PF_6]$ IPC revealed the importance of coordination structures in ion transport by comparing the ion hopping models for Li^+ (cooperative motion between the metal ion and a triangular solvation shell) and Na^+ (interchange between a tetrahedral and triangular solvation shell coordination geometry).[309] Another molecular dynamics simulation on the $[N_{1111}][N(CN)_2]$ IPC proposed doping the IPC phase with Li-ions results in a cluster formation between Li^+ and $N(CN)_2^-$, thus restricting the rotation of $N(CN)_2^-$. This in turn increases the free volume and the defect paths, thereby enhancing ion conduction.[310] More practically, galvanostatic polarization causes a Li^+-concentration gradient between two electrodes. Further, the increase in Li^+ concentration induces an expansion of mobile boundary domains, enhancing the interface of Li^+ mobility as was detected by an in situ magnetic resonance imaging study on the Li[FSA]-$[P_{1i4i4i4}][FSA]$ IPC.[122]

5.3 Applications in lithium secondary batteries

The application of IPCs in Li secondary batteries has been intensively studied, commencing from the report on the Li[TFSA]-$[C_2C_1pyrr][TFSA]$ IPC system.[303] Early studies mainly

discussed ion transport in the IPC phase doped with Li^+ as mentioned above.[302-304,311-314] The thermal behaviour of IPC-forming salts were noted to typically change with the addition of a Li salt.[255,300,312] The disappearance, appearance and shifting of some solid-solid transition peaks were observed to occur depending on the doping degree – an indication that a solid-solution phase was being formed.[124,126,255,305,312,313,315] X-ray diffraction, NMR, and DSC analyses on the Li[BF_4]-[C_2C_1pyrr][BF_4] system revealed a complicated multi-phase behaviour at low temperatures. The analyses further showed that the highest temperature phases engendered a rock-salt structure regardless of the doping amount of Li[BF_4] (0, 10, and 20 mol%) due to the formation of a solid-solution phase.[126]

As shown in Fig. 12a, appropriate cation and anion combinations yield reversible Li metal deposition/dissolution with high efficiencies (Ni electrode in 5 mol% Li[CF_3BF_3]-[N_{1223}][CF_3BF_3] at 25 °C,[255] Pt electrode in 5 mol% Li[BF_4]-[C_2C_1pyrr][BF_4] at 100 °C,[315] Cu electrode in 4 mol% Li[FSA]-[$P_{1i4i4i4}$][FSA] at 100 °C,[124] stainless steel electrode in 0.15 mol kg^{-1} Li[TFSA]-[$C_6(N_{222})_2$][TFSA] at 90 °C,[269] Ni electrode in 5 mol% Li[FSA]-[C_2C_2pyrr][FSA] at 60 °C,[300] and Pt electrode in 10 mol% Li[TFSA]-[N_{1222}][TFSA] at 50 °C[275]). Galvanostatic cycling performed on a Li/Li symmetric cell containing 1 mol% Li[TFSA]-[C_2C_1pyrr][TFSA] IPC manifested a sharp decrease in polarization due to the diminished bulk and interfacial resistances, as demonstrated by EIS measurements – an affirmation of the importance of preconditioning for the cells using IPC electrolytes.[316,317] The IPC phases (Li[BF_4]-[C_1C_1pyrr][BF_4] and Li[BF_4]-[C_2C_1pyrr][BF_4]) targeting operations at intermediate temperatures provided similar results at higher temperatures (90 °C for 8 mol% Li[BF_4]-[C_1C_1pyrr][BF_4] and 70 °C and 80 °C for 10 mol% Li[BF_4]-[C_2C_1pyrr][BF_4] with over 700 cycles were achieved in the latter case).[289,315] In a subsequent report, the resistance was seen to mainly occur from the interface during the initial preconditioning process but with progressive cycling, the participation of the bulk electrolyte gradually increased, eventually becoming the dominant contributor to the resistance in the steady state.[318]

To further ascertain the behaviour of IPC electrolytes, multiple studies employing different types of IPCs and typical electrode materials in the assembly of half-and full-cells have been reported. For instance, a $Li_4Ti_5O_{12}$/$LiFePO_4$ cell containing 10 mol% Li[TFSA]-[$DEMPyr_{123}$][TFSA] IPC exhibited a stable charge-discharge behaviour with a discharge capacity of 114 mAh (g-$LiFePO_4$)$^{-1}$ and a coulombic efficiency of 87 %. Even so, the rate performance was noted to be inferior to that of the [DEPyr][TFSA]-based IL electrolyte.[304] In another probe, a Li/$LiFePO_4$ cell with 10 mol% Li[TFSA]-[C_2C_1pyrr][TFSA] confirmed stable charge-discharge at 0.2C over 100 cycles with a continuous capacity fading at 80 °C.[317,318] (analogous data at 50 °C). This study clearly showed that charge-discharge performance depended on the separators mainly due to the differences in their wettability. Another example of charge-discharge for the Li/$LiFePO_4$ cell was reported at 0.1C with 10 mol% Li[BF_4]-[C_2C_1pyrr][BF_4] at 80 and 100 °C (capacities of 120-140 mAh g^{-1} at 100 °C).[315] The Li/$LiFePO_4$ cell using the 0.5 mol kg^{-1} Li[$N(CN)_2$]-[C_1C_1pyrr][$N(CN)_2$] IPC was charged-discharged at 80 °C, retaining more than 140 mAh g^{-1} in the 200th cycle at 0.1 C.[184] Introduction of the 4 mol% Li[FSA]-[$P_{1i4i4i4}$][FSA] IPC resulted in a highly improved rate performance of the Li/$LiFePO_4$ cell at 20 °C (Phase II) and 30 °C (Phase I), attaining 160 mAh g^{-1} at 0.1 C in both phases, and 118 mAh g^{-1} and 130 mAh g^{-1} at 1C in Phase II and Phase I, respectively.[124]

The concept of "plastic crystal in salt" was also proposed as in the case of “solvent in salt”[319] or “polymer in salt”.[320-322] The quasi-solid state material formed by incorporating 90 mol% Li[FSA] with 10 mol% the [C_2C_2pyrr][FSA] IPC was found to contain two environments of Li^+ (Li[FSA]-rich phase and ion-mobile phase) as depicted by Fig. 12b,c, and exhibited a substantial ionic conductivity (0.24 mS cm^{-1} at 30 °C) along with a high Li^+ transference number of 0.68. The stable Li metal deposition/dissolution behaviour in this material holds enormous promise for a wide range of applications. Many more research avenues have been explored in this direction, for instance, IPCs using [hexamethylguanidinium][FSA] salt combined with Li[FSA] or Li[TFSA], and those using [N_{1222}][TFSA] combined with Li[TFSA], were found to attain promising performance in lithium secondary batteries.[275,305]

5.4 Applications in sodium secondary batteries

The fascinating thermal conductivity and ion transport properties observed in IPCs has also prompted explorations into Na analogues for possible application as electrolytes in Na secondary batteries. Although the literature on these electrolytes is still limited, reports pertaining to the thermal, conductivity, and ion transport properties of Na-based IPC systems have shown similar trends to those containing Li salts.[119,142,323-326] For instance, the Na[TFSA]-[C_2C_1pyrr][TFSA][323] and Na[TFSA]-[P_{111i4}][TFSA] systems[119] exhibit an increase in ionic conductivity upon the addition of Na, depending on the temperature range. On the other hand, only a limited change is observed in the Na[$N(CN)_2$]-[C_1C_1pyrr][$N(CN)_2$] system.[324] The different properties of the Na-rich phase may also produce different behaviour in their ionic conductivity. At 50 °C, the Na[TFSA]-[P_{111i4}][TFSA] system achieved physical and electrochemical properties sufficient for extended electrochemical tests, even though only small amounts of IL were present at this temperature. Besides, the Na^+ transference number of the 25 mol% Na[TFSA]-[P_{111i4}][TFSA] IPC at 50 °C was determined to be 0.39 – a value significantly larger than that of the IL electrolytes.[5,137,327] Additionally, this IPC system sufficiently achieved reversible Na metal deposition-dissolution on a Cu electrode as well as extended cycling of the Na/Na cells at 50 °C. A Na/$NaFePO_4$ cell with the 25 mol% Na[TFSA]-[P_{111i4}][TFSA] IPC was also found to attain a high efficiency coupled with a discharge capacity of 76 mAh g^{-1} at the current rate of 0.1C at 50 °C. Further electrochemical tests were also performed on this Na[FSA]-[$P_{1i4i4i4}$][FSA] system at the Na[FSA] weight ratios of 60 mol% and 90 mol%.[325] The two compositions demonstrated the existence of the liquid phase as well as a time-dependent variation of ionic conductivity, despite the solid-like nature of the materials. The Na/Na symmetric cells containing the 60 mol% Na[FSA] achieved stable cycling at 50 °C and room temperature while the symmetric cells containing 90

mol% Na[FSA] were stably cycled at 90 °C and 50 °C. The results observed in the (pseudo-) solid-state electrolytes with high Na salt ratios demonstrate a potential to mitigate various challenges in battery operations by varying the constituent salt concentrations.

The effects of anionic structures on the properties of Na-salt containing $[P_{1i4i4i4}][FSA]$ have also been reported.[142] The addition of $Na[PF_6]$ was found to result in the appearance of new phases, whereas the addition of Na[FSA] and Na[TFSA] produced a wide-ranged liquid-phase composition. Another report on the effects of ionic structures with the Na[FSA]-$[P_{1i4i4i4}][FSA]$, Na[TFSA]-$[P_{1i4i4i4}][TFSA]$, and Na[TFSA]-$[P_{111i4}][TFSA]$ systems at the Na salt ratio of 70 mol% suggested that combining phosphonium cations with smaller alkyl chains in combination with a smaller anions produced lower melting points, higher conductivities, with a higher current response during Na metal deposition/dissolution tests.[326] In another study on the practicality of electrodes for Na secondary batteries, the 90 mol% Na[FSA]-$[P_{1i4i4i4}][FSA]$ IPC at 60 °C was examined alongside $Na_3V_2(PO_4)_3$ and $Na_2FeP_2O_7$ positive electrode materials (Fig. 12d). These two electrode materials, which are well-studied for their use with IL electrolytes, were found to achieve a high performance at intermediate temperatures in the IPC system.[328-331] As mentioned above, even though the 90 mol% Na[FSA]-$[P_{1i4i4i4}][FSA]$ IPC contains a small amount of liquid phase, it is still considered a solid-state electrolyte even at 60 °C (ionic conductivity: 0.56 mS cm^{-1}). As expected, ion transport and electron transfer are improved by the temperature elevation, yielding high rate and cycle performances for both electrodes (e.g., 72 mAh g^{-1} at 1C and 96 % retention after 60 cycles for $Na_3V_2(PO_4)_3$).

5.5 Composite with polymer

Despite the propitious performance of IPCs, their low mechanical strength remains a limiting factor to their practicality for diverse battery operations. Efforts to address this issue has driven immense focus into the exploration of composite electrolytes comprising polymers and IPCs to form free-standing films. Early works on Li[BF_4]-[C_3C_1pyrr][BF_4]-PEO or PVP composites revealed ionic conductivity decreases when a polymer is added to the plastic crystal phase, in contrast with the pure IPC (without Li[BF_4]) phase, which shows a different behaviour depending on the blended polymer.[312,332] In previous works, some full cell test data with IPCs were obtained using a polymer separator, as mentioned in the previous section.[317,318] In a bid to advance the practicality of the IPC electrolytes, attempts were made to fabricate IPC films using more functional polymers. So far, PVDF has been the most popular polymer applied for this purpose. In a study on the effects of a polymer surface on the ionic conductivities of a pure IPC using PVDF and PS; the formation of a conductive structure on the surface was determined to be an important factor for ion transport.[333] A PVDF fibre impregnated with 10 mol% Li[BF_4]-[C_3C_1pyrr][BF_4] IPC forms a thin and flexible film that exhibits a higher ionic conductivity than that of the IPC on its own.[129,334] The PVDF composite is considered an expansion of the IPC lattice and thus enhances the cation mobility. The $LiFePO_4$ electrode delivers a discharge capacity of 140 mAh g^{-1} at 80 °C, with a steady increase in capacity from the 1st (around 100 mAh g^{-1}) to the 8th cycle. Another type of PVDF composite with the Li[BF_4]-[C_3C_1pyrr][BF_4] IPC prepared through co-electrospinning exclusively, was found to contain the electroactive β-phase PVDF which exhibited an improved ionic conductivity.[128] Likewise, FSA^--based IPCs with PVDF fibre provided superior performance when used with certain positive electrode materials. For instance, 10 mol% Li[FSA]-[C_2C_1pyrr][FSA] IPC with PVDF fibres attained a 520-cycle Li metal deposition-dissolution in the Li/Li symmetric cell at both ambient temperatures and 50 °C with a gradual decrease in polarization observed.[335] Increasing Li[FSA] in the same IPC system to 50 mol% resulted in the formation of an amorphous IPC phase with PVDF fibre along with an increase in ionic conductivity.[336] The Li/Li symmetric cell with the 8 wt% PVdF-92 wt % IPC (50 mol% Li[FSA]-[C_2C_1pyrr][FSA]) composite achieved 500-cycle Li metal deposition/dissolution at 50 °C but resulted in a short-circuit after 250 cycles at 23 °C due to an invariable Li metal dendrite formation. On the grounds of the excellent stability of Al electrodes at high potentials, as has been confirmed in this system as well as analogous IL electrolytes,[337] a high-potential positive electrode material, $LiNi_{1/3}Mn_{1/3}Co_{1/3}O_2$, was examined alongside an Al electrode. The resulting data showed a continuous decrease in discharge capacities from 120 mAh g^{-1} at the 1st cycle to about 80 mAh g^{-1} at the 78th cycle at 1/15C with coulombic efficiencies mostly above 90 %. However, combining PVDF nano-particles with the Li[FSA]-[C_2C_1pyrr][FSA] system was found to result in a composite with a higher ratio of PVDF than typical composites containing PVDF fibres, thereby producing different physical and electrochemical properties.[120,338] The Improved ionic conductivity of the 60 wt% PVDF-40 wt % IPC (10 mol% Li[FSA]-[C_2C_1pyrr][FSA]) composite yielded a high rate (119 mAh g^{-1} at 2 C after 100 cycles at 50 °C) and excellent cycle performances (coulombic efficiency of 99.8% at 2 C after 1200 cycles at room temperature) from the Li/$LiFePO_4$ cell. Similarly, the IPC composite delivered a stable charge-discharge performance in the Li/$LiNi_{1/3}Mn_{1/3}Co_{1/3}O_2$ cell. A further increase of Li[FSA] (the 60 wt% PVDF-40 wt % IPC (50 mol% Li[FSA]-[C_2C_1pyrr][FSA]) composite) lead to an even more stable electrochemical behaviour in the Li/$LiNi_{1/3}Mn_{1/3}Co_{1/3}O_2$ cell over 1300 cycles (Fig. 12e,f).

Composite electrolytes utilizing other polymers alongside IPCs have also be explored for lithium batteries. The Li/$LiFePO_4$ cells with the composites comprising a polymer and Li-containing IPCs ([A][339] PEO : Li[FSA] : [C_2C_1pyrr][FSA] = 57.7 : 12.3 : 30, [B] PEO : Li[FSA] : [N_{1222}][FSA] = 57.7 : 12.3 : 30),[340] and [C][287] P(VDF-HFP) : Li[FSA] : [N_{1222}][FSA] = 16 : 20 : 64 in weight) exhibited stable cycling at 50 °C, delivering discharge capacities of 150.3 mAh g^{-1} after 90 cycles for [A], 151.5 mAh g^{-1} after 120 cycles for [B], and 150.5 mAh g^{-1} after 100 cycles for [C] at 0.2C. These results suggest a high compatibility of FSA-based IPCs with a variety of polymers. Nonetheless, it should be noted that Piperidinium-based IPCs have been less intensively investigated than those based on pyrrolidinium.

The [C_2C_1pip][FSA] salt combined with Li[FSA] has a remarkably wide IPC temperature range as well as a high ionic

conductivity.[341] A Li/$LiFePO_4$ cell using the flexible P(VDF-HFP)-based composite (P(VDF-HFP) : Li[FSA] : $[C_2C_1pip][FSA]$ = 22.44 : 10.23 : 67.33 in weight) achieved protracted cycling at 0.2C, and a discharge capacity of 137.2 mAh g^{-1} after 500 cycles at 25 °C. Similarly, a Li/$LiNi_{0.6}Co_{0.2}Mn_{0.2}O_2$ cell cycled at 1.0C in the same electrolyte system achieved a discharge capacity of 152.6 mAh g^{-1} after 100 cycles at 25 °C. The introduction of a dendrimer, a hyperbranched bismethylolpropionic acid polymer or generation 4, into the Li[BF_4]-$[C_2C_1pyrr][BF_4]$ system disrupted the ordering of the OIPC phase and shifted the transition temperatures to lower values.[342] However, it is worthy to note that the addition of these compounds only improves the ionic conductivities of the Li[BF_4]-$[C_2C_1pyrr][BF_4]$ system and does not enhance those of the $[C_2C_1pyrr][BF_4]$ electrolyte. The presence of the dendrimer prevents crystallization of Li-rich phases at low temperatures, although the structure of the highest temperature phase does not change.

The incorporation of polymeric IL with IPCs has also been found to produce a self-standing conductive film (see Fig. 12b). The composite material of polymeric IL and IPC ([P(DADMA)][TFSA] : $[C_2C_1pyrr][FSA]$: Li[TFSA] = 40 : 40 : 20 in weight) exhibited the highest ionic conductivity among the examined compositions. The discharge capacity of the Li/$LiFePO_4$ cell cycled at 0.2C was noted to increase with temperature elevations, attaining 160 mAh g^{-1} after 150 cycles at 80 °C.[127] The same polymeric IL also forms a conductive film with the $[N_{1222}][FSA]$-Li[TFSA] IPC, which acts as an electrolyte for the Li/$LiFePO_4$ cell.

The excellent thermal and physicochemical properties of IPC electrolytes promise to raise the safety thresholds of secondary batteries. However, their conductivities remain lower than the other types of electrolytes – a major challenge to their advancement. However, the myriads of combinations coupled with the auspicious tuneability presented in this minireview predict their imminent prosperity in future batteries.

6. Summary, Future Perspective and Challenges

In this minireview, we provide a systematic description of pseudo-solid-state electrolytes prepared using ILs. For a clear perspective on the recent progress and future direction of these materials, our literature survey highlighted the need to split the pseudo-solid-state electrolytes into three classes: hybrid, ionogel, and IPC. Solid-state electrolytes are envisioned to be the prime materials of choice in the design of next-generation rechargeable batteries. However, their current utilisation is heavily mired by severe dendrite formation and high interfacial resistances. As a measure, we focus on incorporating ILs or related compounds to improve various aspects of battery performance. The pseudo-solid-state electrolytes are noted to deliver better performance than solid-state electrolytes, owing to the presence of a liquid or flexible solid phase in limited amounts.

In comparison to the organic solvent electrolytes, ILs are better poised to bring out the superior qualities of solid-state electrolytes due to their exceptional properties such as low volatility, low flammability, high tolerance for high temperatures, among other exquisite electrochemical capabilities. In hybrid solid-state electrolytes, the ILs serve as subordinate ion conductors, working in tandem with the solid-state electrolytes, which serve as the prominent ion conductors. Even so, the ILs are still essential in enhancing the interfacial properties of the electrolyte (see Figures 4, 5, and 6 for selected examples) and suppressing Li metal dendrite formation. In fact, some hybrid solid-state electrolytes have been reported to exhibit reduced interfacial resistance with extended cyclabilities of over 10000 cycles.

Herein, we also delve into the use of ILs in ionogels. This class of pseudo-solid-state electrolytes comprises an inorganic (in some cases organic) solid matrix hosting an IL. The solid framework not only enhances the ion transport properties of the IL but also augments their mechanical strength while preserving the unique characteristics and electrochemical performance of ILs (see Figures 7, 8, and 9). Reports on Li symmetric cells employing ionogels alongside common electrode materials have demonstrated stable cycling in a wide temperature range, evincing the high potential of this class of pseudo-solid-state electrolytes. To derive high performance from these electrolytes, the formulation of homogenous ionogels can be instrumental in enhancing their wettability. Further, for the practical application of ionogels in future rechargeable batteries, their long-term compatibility with electrode materials should also be explored to prevent detrimental side reactions within the cells.

Still in the line of pseudo-solid-state electrolytes, we explore the prospects of IPC electrolytes in rechargeable batteries. IPCs constitute a class of crystalline materials with unique ion transport properties complemented by high flexibility and plasticity. It should be noted that IPCs can function as solid-state electrolytes independently or can be used together with polymers to form composite electrolytes (PILs frames). However, this minireview covers these materials for their close resemblance to pseudo-solid-state electrolytes fabricated using ILs. In any case, IPC electrolytes deliver high performance as secondary battery electrolytes. For instance, reports on the charge-discharge behaviour of IPC electrolytes (in some cases IPC and polymer composites) used alongside various electrode materials demonstrated long cycling of over 1000 cycles with a metal oxide positive electrode. Exploration into their physical states (i.e., phase behaviour and their static and dynamic phases for ion transport) not only draws fundamental interest but also presents new ways of tuning their performance, such as through doping with highly concentrated alkali ions. However, inquests into the mechanical properties of IPCs and related materials are still very scarce. Thus, future probes in this direction will be vital to improving their practicality.

Based on the scope of this minireview, IL electrolytes are veritably superior to their organic solvent counterparts, validating their use in the formulation of pseudo-solid-state electrolytes. The ionically dense fields created by ILs-based materials not only enhance the concentration of charge-carrying ions but also aid in unlocking other fascinating physical and chemical behaviour in solid-state electrolytes. For insight into the future of pseudo-solid-state electrolytes, we take a

closer look into the three categories (hybrid, ionogel, and IPC) presented herein. In the hybrid solid-state systems, ion transport is mainly facilitated by the solid-state electrolytes, while ILs play a subordinate role. Given that ceramic-based solid-state electrolytes are already well-established in state-of-the-art batteries, incorporating existing ILs would be a straightforward route for developing this class of pseudo-solid-state electrolytes. As for ionogels, the ILs serve as the principal ion conductors while the host matrices provide structural support. Although the host matrices significantly contribute to the entire electrochemical performance of the system, the choice of the IL is more crucial in determining the general parameters of the ionogels electrolytes. As such, the performance of these systems hinges on advancements in IL electrolytes. Please note that some host materials tend to be very expensive, which may hinder the commercialisation of ionogel-based batteries; thus, economic discretion would be recommended. Finally, the IPC class of pseudo-solid-state electrolytes may require a protracted timescale to achieve practical utility. Despite their superb mechanical, thermal, electrochemical and ion transport properties, their underlying mechanisms are incomparable to other existing solid-state electrolytes. Nonetheless, IPCs can be used in conjunction with inorganic or polymer materials to form composites with high mechanical properties, thereby suppressing leakage problems. With this approach, already developed fabrication methods for ionogels can be employed to cut their development time.

Accordingly, other components such as the ion conductors in hybrid solid-state electrolytes, host materials in ionogels, and ion structures of ILs or IPCs will also need further optimisation to propel this field to the next level. Certainly, this will require both experimental and theoretical efforts at molecular levels to gain academic insights, in particular, on the interfacial properties from the viewpoints of physical, electrochemical, and material chemistries. Besides, such inquest might also reveal previously unknown functionalities derived by the introduction of ILs. Indeed, there is no "silver bullet" for the prevalent issue among current battery systems but the pseudo-solid-state class of electrolytes offers a glimmer of what their future holds.

Conflicts of interest

There are no conflicts to declare

Abbreviations

$C_6(N_{222})_2^+$: *N*,*N*,*N*,*N*′,*N*′,*N*′-hexaethyl-1,6-hexanediammonium
$C_nC_n$pyr$^+$ = *N*,*N*-dialkylpyrazolium (*n*: number of carbon atoms in alkyl chain)
$C_nC_n$pip$^+$: *N*,*N*-dialkylpiperidinium (*n*: number of carbon atoms in alkyl chain)
$C_nC_n$im$^+$: 1,3-dialkylimidazolium (*n*: number of carbon atoms in alkyl chain)
$C_nC_n$pyrr$^+$: *N*,*N*-dialkylpyrrolidinium (*n*: number of carbon atoms in alkyl chain)
AC_1im^+: 1-allyl-3-methylimidazolium
$DEMPyr_{123}^+$: *N*,*N*′-diethyl-3-methylpyrazolium
DEPyr$^+$: *N*,*N*′-diethylpyrazolium
DSC: differential scanning calorimetry
EDS: energy dispersive X-ray spectroscopy
EIS: electrochemical impedance spectroscopy
FSA$^-$: bis(fluorosulfonyl)amide / FSI$^-$: bis(fluorosulfonyl)imide
G3: triglyme
G4: tetraglyme
hBN: hexagonal boron nitride
IL: ionic liquid
IPC: Ionic plastic crystal
LIB: Li-ion battery
LLZO: $Li_7La_3Zr_2O_{12}$
MOF-525(Cu): $Zr_6O_4(OH)_4$(TCPP-Cu)$_3$; (TCPP = 5,10,15,20-tetrakis(4-carboxyphenyl)porphyrin)
NMR: Nuclear magnetic resonance
NASICON: Na super ionic conductor
N_{nnnn}^+: tetraalkylammonium (n: number of carbon atom in alkyl chain)
PIL: polymeric ionic liquid
P(DADMA): poly(diallyldimethylammonium)
PCP: porous coordination polymer
PEO: Polyethylene glycol
PVP: poly(vinyl pyrrolidone)
PVDF: poly(vinylidene fluoride)
PS: polystyrene
P(VDF-HFP): poly(vinylidene fluoride-co-hexafluoropropylene)
P_{122i4}^+: diethylmethylisobutylphosphonium
P_{nnnn}^+: tetraalkylphosphonium (n: number of carbon atom in alkyl chain or i4 = isobutyl)
SEM: scanning electron microscopy
TEMMP$^+$: Triethyl(methoxymethyl)phosphonium
TFSA$^-$: bis(trifluoromethylsulfonyl)amide
TGA: thermogravimetric analysis
XRD: X-ray diffraction
ZIF-8: Zn(MeIM)$_2$; H(MeIM) = 2-methylimidazole

Acknowledgements

This study was partly supported by the Japan Society for the Promotion of Science (JSPS, KAKENHI Grant Number 19H02811) and Collaborative Laboratory for System Design of Solid Type Battery, Department of Energy and Hydrocarbon Chemistry, Graduate School of Engineering, Kyoto University.

Notes and reference

1. D. Larcher and J. M. Tarascon, *Nat. Chem.*, 2015, **7**, 19-29.
2. M. Armand and J. M. Tarascon, *Nature*, 2008, **451**, 652-657.
3. T. M. Bandhauer, S. Garimella and T. F. Fuller, *J. Electrochem. Soc.*, 2011, **158**, R1.
4. C.-Y. Chen, K. Matsumoto, K. Kubota, R. Hagiwara and Q. Xu, *Adv. Funct. Mater.*, 2020, **30**, 2003557.
5. K. Matsumoto, J. Hwang, S. Kaushik, C.-Y. Chen and R. Hagiwara, *Energy Environ. Sci.*, 2019, **12**, 3247-3287.
6. J. Ming, J. Guo, C. Xia, W. Wang and H. N. Alshareef, *Mater. Sci.*

Eng. R Rep., 2019, **135**, 58-84.
7. Y. Zhang, Z. Chen, H. Qiu, W. Yang, Z. Zhao, J. Zhao and G. Cui, *NPG Asia Mater.*, 2020, **12**, 4.
8. R. Rajagopalan, Y. Tang, X. Ji, C. Jia and H. Wang, *Adv. Funct. Mater.*, 2020, **30**, 1909486.
9. T. Hosaka, K. Kubota, A. S. Hameed and S. Komaba, *Chem. Rev.*, 2020, **120**, 6358-6466.
10. W. Zhang, Y. Liu and Z. Guo, *Sci. Adv.*, 2019, **5**, eaav7412.
11. J. Y. Hwang, S. T. Myung and Y. K. Sun, *Chem. Soc. Rev.*, 2017, **46**, 3529-3614.
12. M. K. Aslam, Y. Niu and M. Xu, *Adv. Energy Mater.*, 2021, **11**, 2000681.
13. D.-T. Nguyen, R. Horia, A. Y. S. Eng, S.-W. Song and Z. W. Seh, *Mater. Horiz.*, 2021, **8**, 830-853.
14. M. Mao, T. Gao, S. Hou and C. Wang, *Chem. Soc. Rev.*, 2018, **47**, 8804-8841.
15. Z. Ma, X. Yuan, L. Li, Z.-F. Ma, D. P. Wilkinson, L. Zhang and J. Zhang, *Energy Environ. Sci.*, 2015, **8**, 2144-2198.
16. X. Cai, L. Lai, J. Lin and Z. Shen, *Mater. Horiz.*, 2017, **4**, 945-976.
17. Z. W. Seh, Y. Sun, Q. Zhang and Y. Cui, *Chem. Soc. Rev.*, 2016, **45**, 5605-5634.
18. R. Fang, J. Xu and D.-W. Wang, *Energy Environ. Sci.*, 2020, **13**, 432-471.
19. A. M. Haregewoin, A. S. Wotango and B.-J. Hwang, *Energy Environ. Sci.*, 2016, **9**, 1955-1988.
20. B. Scrosati, J. Hassoun and Y.-K. Sun, *Energy Environ. Sci.*, 2011, **4**, 3287-3295.
21. R. Murugan, V. Thangadurai and W. Weppner, *Angew. Chem., Int. Ed.*, 2007, **46**, 7778-7781.
22. N. Kamaya, K. Homma, Y. Yamakawa, M. Hirayama, R. Kanno, M. Yonemura, T. Kamiyama, Y. Kato, S. Hama, K. Kawamoto and A. Mitsui, *Nat. Mater.*, 2011, **10**, 682-686.
23. F. Li, H. Kitaura and H. Zhou, *Energy Environ. Sci.*, 2013, **6**, 2302-2311.
24. R. Chen, W. Qu, X. Guo, L. Li and F. Wu, *Mater. Horiz.*, 2016, **3**, 487-516.
25. F. Zheng, M. Kotobuki, S. Song, M. O. Lai and L. Lu, *J. Power Sources*, 2018, **389**, 198-213.
26. J. F. M. Oudenhoven, L. Baggetto and P. H. L. Notten, *Adv. Energy Mater.*, 2011, **1**, 10-33.
27. K. Yamamoto, M. Takahashi, K. Ohara, N. H. H. Phuc, S. Yang, T. Watanabe, T. Uchiyama, A. Sakuda, A. Hayashi, M. Tatsumisago, H. Muto, A. Matsuda and Y. Uchimoto, *ACS Omega*, 2020, **5**, 26287-26294.
28. M. Takahashi, S. Yang, K. Yamamoto, K. Ohara, N. H. H. Phuc, T. Watanabe, T. Uchiyama, A. Sakuda, A. Hayashi, M. Tatsumisago, H. Muto, A. Matsuda and Y. Uchimoto, *Solid State Ionics*, 2021, **361**, 115568.
29. L. Fan, S. Li, L. Liu, W. Zhang, L. Gao, Y. Fu, F. Chen, J. Li, H. L. Zhuang and Y. Lu, *Adv. Energy Mater.*, 2018, **8**, 1802350.
30. Z. Zhang, Q. Zhang, J. Shi, Y. S. Chu, X. Yu, K. Xu, M. Ge, H. Yan, W. Li, L. Gu, Y.-S. Hu, H. Li, X.-Q. Yang, L. Chen and X. Huang, *Adv. Energy Mater.*, 2017, **7**, 1601196.
31. S. Xiong, Y. Liu, P. Jankowski, Q. Liu, F. Nitze, K. Xie, J. Song and A. Matic, *Adv. Funct. Mater.*, 2020, **30**, 2001444.
32. Q.-C. Liu, J.-J. Xu, S. Yuan, Z.-W. Chang, D. Xu, Y.-B. Yin, L. Li, H.-X. Zhong, Y.-S. Jiang, J.-M. Yan and X.-B. Zhang, *Adv. Mater.*, 2015, **27**, 5241-5247.
33. W. Tang, X. Yin, S. Kang, Z. Chen, B. Tian, S. L. Teo, X. Wang, X. Chi, K. P. Loh, H.-W. Lee and G. W. Zheng, *Adv. Mater.*, 2018, **30**, 1801745.
34. S. Seki, Y. Kobayashi, H. Miyashiro, Y. Ohno, A. Usami, Y. Mita, M. Watanabe and N. Terada, *Chem. Commun.*, 2006, DOI: 10.1039/b514681j, 544-545.
35. S. Tian, B. Shao, Z. Wang, S. Li, X. Liu, Y. Zhao and L. Li, *Chin. Chem. Lett.*, 2019, **30**, 1289-1292.
36. H. Kim, Y. Ding and P. A. Kohl, *J. Power Sources*, 2012, **198**, 281-286.
37. S. A. Pervez, B. P. Vinayan, M. A. Cambaz, G. Melinte, T. Diemant, T. Braun, G. Karkera, R. J. Behm and M. Fichtner, *J. Mater. Chem. A*, 2020, **8**, 16451-16462.
38. S. A. Pervez, G. Kim, B. P. Vinayan, M. A. Cambaz, M. Kuenzel, M. Hekmatfar, M. Fichtner and S. Passerini, *Small*, 2020, **16**, 2000279.
39. H. W. Kim, P. Manikandan, Y. J. Lim, J. H. Kim, S.-c. Nam and Y. Kim, *J. Mater. Chem. A*, 2016, **4**, 17025-17032.
40. W. Zhang, X. Wang, Q. Zhang, L. Wang, Z. Xu, Y. Li and S. Huang, *ACS Appl. Energy Mater.*, 2020, **3**, 5238-5246.
41. E. J. Cheng, T. Kimura, M. Shoji, H. Ueda, H. Munakata and K. Kanamura, *ACS Appl. Mater. Interfaces*, 2020, **12**, 10382-10388.
42. Y. Cao, S. Lou, Z. Sun, W. Tang, Y. Ma, P. Zuo, J. Wang, C. Du, Y. Gao and G. Yin, *Chem Eng J*, 2020, **382**, 123046.
43. P. Schmitz, M. Kolek, M. Pyschik, K. Jalkanen, S. Nowak, M. Winter and P. Bieker, *Chemistryselect*, 2017, **2**, 6052-6056.
44. P. Schmitz, R. Jakelski, M. Pyschik, K. Jalkanen, S. Nowak, M. Winter and P. Bieker, *ChemSusChem*, 2017, **10**, 876-883.
45. X. Cai, B. Ye, J. Ding, Z. Chi, L. Sun, P. Saha and G. Wang, *J. Mater. Chem. A*, 2021, **9**, 2459-2469.
46. C. de la Torre-Gamarra, G. B. Appetecchi, U. Ulissi, A. Varzi, A. Varez and S. Passerini, *J. Power Sources*, 2018, **383**, 157-163.
47. K.-N. Gao, H.-R. Wang, M.-H. He, Y.-Q. Li, Z.-H. Cui, Y. Mao and T. Zhang, *J. Power Sources*, 2020, **463**, 228179.
48. S. Xiong, K. Xie, E. Blomberg, P. Jacobsson and A. Matic, *J. Power Sources*, 2014, **252**, 150-155.
49. J. Kawaji, A. Unemoto, T. Hirano, D. Takamatsu, E. Seki, M. Morishima and T. Okumura, *J. Electrochem. Soc.*, 2020, **167**, 140525.
50. F. Sagane, T. Abe and Z. Ogumi, *J. Electrochem. Soc.*, 2012, **159**, A1766-A1769.
51. J. Saint, A. S. Best, A. F. Hollenkamp, J. Kerr, J. H. Shin and M. M. Doeff, *J. Electrochem. Soc.*, 2008, **155**, A172.
52. W. Liu, F. Deng, S. Song, G. Ji, N. Hu and C. Xu, *Mater. Technol.*, 2020, **35**, 618-624.
53. J.-Y. Park, J.-W. Park, C.-H. Doh, Y.-C. Ha, S.-M. Lee and S. Kim, *Res. Chem. Intermed.*, 2018, **44**, 6039-6051.
54. A. Unemoto, Y. Gambe, D. Komatsu and I. Honma, *Solid State Ionics*, 2014, **262**, 765-768.
55. B. Zheng, J. Zhu, H. Wang, M. Feng, E. Umeshbabu, Y. Li, Q.-H. Wu and Y. Yang, *ACS Appl. Mater. Interfaces*, 2018, **10**, 25473-25482.
56. D. Y. Oh, Y. J. Nam, K. H. Park, S. H. Jung, S.-J. Cho, Y. K. Kim, Y.-G. Lee, S.-Y. Lee and Y. S. Jung, *Adv. Energy Mater.*, 2015, **5**, 1500865.
57. B. Sun, K. Liu, J. Lang, M. Fang, Y. Jin and H. Wu, *Electrochim. Acta*, 2018, **284**, 662-668.
58. M. Falco, L. Castro, J. R. Nair, F. Bella, F. Bardé, G. Meligrana and C. Gerbaldi, *ACS Appl. Energy Mater.*, 2019, **2**, 1600-1607.
59. M. Falco, C. Simari, C. Ferrara, J. R. Nair, G. Meligrana, F. Bella, I. Nicotera, P. Mustarelli, M. Winter and C. Gerbaldi, *Langmuir*, 2019, **35**, 8210-8219.
60. J. S. Wilkes, *Green Chemistry*, 2002, **4**, 73-80.
61. P. Wasserscheid and W. Keim, *Angew. Chem. Int. Ed.*, 2000, **39**, 3772-3789.

62. R. Hagiwara and Y. Ito, *J. Fluorine Chem.*, 2000, **105**, 221-227.
63. T. Welton, *Chem. Rev.*, 1999, **99**, 2071-2084.
64. R. Hagiwara and J. S. Lee, *Electrochemistry*, 2007, **75**, 23-34.
65. M. Watanabe, M. L. Thomas, S. Zhang, K. Ueno, T. Yasuda and K. Dokko, *Chem. Rev.*, 2017, **117**, 7190-7239.
66. M. Galiński, A. Lewandowski and I. Stępniak, *Electrochim. Acta*, 2006, **51**, 5567-5580.
67. D. Monti, E. Jonsson, M. R. Palacin and P. Johansson, *J. Power Sources*, 2014, **245**, 630-636.
68. N. Wongittharom, C.-H. Wang, Y.-C. Wang, C.-H. Yang and J.-K. Chang, *ACS Appl. Mater. Interfaces*, 2014, **6**, 17564-17570.
69. C. R. Pope, M. Kar, D. R. MacFarlane, M. Armand, M. Forsyth and L. A. O'Dell, *ChemPhysChem*, 2016, **17**, 3187-3195.
70. T. Hosokawa, K. Matsumoto, T. Nohira, R. Hagiwara, A. Fukunaga, S. Sakai and K. Nitta, *J. Phys. Chem. C*, 2016, **120**, 9628-9636.
71. M. Hilder, M. Gras, C. R. Pope, M. Kar, D. R. MacFarlane, M. Forsyth and L. A. O'Dell, *Phys. Chem. Chem. Phys.*, 2017, **19**, 17461-17468.
72. M. Hilder, P. C. Howlett, D. Saurel, E. Gonzalo, A. Basile, M. Armand, T. Rojo, M. Kar, D. R. MacFarlane and M. Forsyth, *Electrochim. Acta*, 2018, **268**, 94-100.
73. C.-H. Wang, Y.-W. Yeh, N. Wongittharom, Y.-C. Wang, C.-J. Tseng, S.-W. Lee, W.-S. Chang and J.-K. Chang, *J. Power Sources*, 2015, **274**, 1016-1023.
74. T. Vogl, C. Vaalma, D. Buchholz, M. Secchiaroli, R. Marassi, S. Passerini and A. Balducci, *J. Mater. Chem. A*, 2016, **4**, 10472-10478.
75. S. A. M. Noor, N. C. Su, L. T. Khoon, N. S. Mohamed, A. Ahmad, M. Z. A. Yahya, H. Zhu, M. Forsyth and D. R. MacFarlane, *Electrochim. Acta*, 2017, **247**, 983-993.
76. H. Yoon, H. Zhu, A. Hervault, M. Armand, D. R. MacFarlane and M. Forsyth, *Phys. Chem. Chem. Phys.*, 2014, **16**, 12350-12355.
77. P. J. Fischer, M. P. Do, R. M. Reich, A. Nagasubramanian, M. Srinivasan and F. E. Kuehn, *Phys. Chem. Chem. Phys.*, 2018, **20**, 29412-29422.
78. S. A. Mohd Noor, P. C. Howlett, D. R. MacFarlane and M. Forsyth, *Electrochim. Acta*, 2013, **114**, 766-771.
79. S. Brutti, M. A. Navarra, G. Maresca, S. Panero, J. Manzi, E. Simonetti and G. B. Appetecchi, *Electrochim. Acta*, 2019, **306**, 317-326.
80. J. Serra Moreno, G. Maresca, S. Panero, B. Scrosati and G. B. Appetecchi, *Electrochem. Commun.*, 2014, **43**, 1-4.
81. M. Hilder, P. C. Howlett, D. Saurel, E. Gonzalo, M. Armand, T. Rojo, D. R. MacFarlane and M. Forsyth, *J. Power Sources*, 2017, **349**, 45-51.
82. W. Xu, J. Wang, F. Ding, X. Chen, E. Nasybulin, Y. Zhang and J.-G. Zhang, *Energy Environ. Sci.*, 2014, **7**, 513-537.
83. X.-B. Cheng, R. Zhang, C.-Z. Zhao and Q. Zhang, *Chem. Rev.*, 2017, **117**, 10403-10473.
84. X.-B. Cheng, R. Zhang, C.-Z. Zhao, F. Wei, J.-G. Zhang and Q. Zhang, *Adv. Sci.*, 2016, **3**, 1500213.
85. A. Basile, A. F. Hollenkamp, A. I. Bhatt and A. P. O'Mullane, *Electrochem. Commun.*, 2013, **27**, 69-72.
86. N. Schweikert, A. Hofmann, M. Schulz, M. Scheuermann, S. T. Boles, T. Hanemann, H. Hahn and S. Indris, *J. Power Sources*, 2013, **228**, 237-243.
87. A. I. Bhatt, P. Kao, A. S. Best and A. F. Hollenkamp, *J. Electrochem. Soc.*, 2013, **160**, A1171-A1180.
88. W. Xu, J. Wang, F. Ding, X. Chen, E. Nasybulin, Y. Zhang and J.-G. Zhang, *Energ. Environ. Sci.*, 2014, **7**, 513-537.
89. I. A. Shkrob, T. W. Marin, Y. Zhu and D. P. Abraham, *J. Phys. Chem. C*, 2014, **118**, 19661-19671.
90. S. A. Alexandre, G. G. Silva, R. Santamaría, J. P. C. Trigueiro and R. L. Lavall, *Electrochim. Acta*, 2019, **299**, 789-799.
91. U. A. Rana, M. Forsyth, D. R. MacFarlane and J. M. Pringle, *Electrochim. Acta*, 2012, **84**, 213-222.
92. B. Asbani, C. Douard, T. Brousse and J. Le Bideau, *Energy Storage Mater.*, 2019, **21**, 439-445.
93. H. Chen, S.-Y. Han, R.-H. Liu, T.-F. Chen, K.-L. Bi, J.-B. Liang, Y.-H. Deng and C.-Q. Wan, *J. Power Sources*, 2018, **376**, 168-176.
94. H. A. Elwan, M. Mamlouk and K. Scott, *J. Power Sources*, 2021, **484**, 229197.
95. N. Yadav, M. K. Singh, N. Yadav and S. A. Hashmi, *J. Power Sources*, 2018, **402**, 133-146.
96. Y. Gao, G. Chen, X. Wang, H. Yang, Z. Wang, W. Lin, H. Xu, Y. Bai and C. Wu, *ACS Appl. Mater. Interfaces*, 2020, **12**, 22981-22991.
97. W. J. Hyun, C. M. Thomas and M. C. Hersam, *Adv. Energy Mater.*, 2020, **10**, 2002135.
98. D. Kim, X. Liu, B. Yu, S. Mateti, L. A. O'Dell, Q. Rong and Y. Chen, *Adv. Funct. Mater.*, 2020, **30**, 1910813.
99. S. Horike, S. S. Nagarkar, T. Ogawa and S. Kitagawa, *Angew. Chem., Int. Ed.*, 2020, **59**, 6652-6664.
100. Y. Li, K.-W. Wong and K.-M. Ng, *Chem. Commun.*, 2016, **52**, 4369-4372.
101. S. Zhang, J. Zhang, Y. Zhang and Y. Deng, *Chem. Rev.*, 2017, **117**, 6755-6833.
102. A. K. Tripathi and R. K. Singh, *J. Energy Storage*, 2018, **15**, 283-291.
103. Z. Wang, Z. Wang, L. Yang, H. Wang, Y. Song, L. Han, K. Yang, J. Hu, H. Chen and F. Pan, *Nano Energy*, 2018, **49**, 580-587.
104. X. Wang, M. Salari, D.-e. Jiang, J. Chapman Varela, B. Anasori, D. J. Wesolowski, S. Dai, M. W. Grinstaff and Y. Gogotsi, *Nat. Rev. Mater.*, 2020, **5**, 787-808.
105. Y. Ren, J. Guo, Z. Liu, Z. Sun, Y. Wu, L. Liu and F. Yan, *Sci. Adv.*, 2019, **5**, eaax0648.
106. B. Joos, T. Vranken, W. Marchal, M. Safari, M. K. Van Bael and A. T. Hardy, *Chem. Mater.*, 2018, **30**, 655-662.
107. M.-A. Néouze, J. Le Bideau, P. Gaveau, S. Bellayer and A. Vioux, *Chem. Mater.*, 2006, **18**, 3931-3936.
108. M. Brachet, D. Gaboriau, P. Gentile, S. Fantini, G. Bidan, S. Sadki, T. Brousse and J. Le Bideau, *J. Mater. Chem. A*, 2016, **4**, 11835-11843.
109. D. Hubble, J. Qin, F. Lin, I. A. Murphy, S.-H. Jang, J. Yang and A. K. Y. Jen, *J. Mater. Chem. A*, 2018, **6**, 24100-24106.
110. K. Ueno, K. Hata, T. Katakabe, M. Kondoh and M. Watanabe, *J. Phys. Chem. C*, 2008, **112**, 9013-9019.
111. M. Forsyth, L. Porcarelli, X. Wang, N. Goujon and D. Mecerreyes, *Accounts Chem Res*, 2019, **52**, 686-694.
112. I. Osada, H. de Vries, B. Scrosati and S. Passerini, *Angew. Chem., Int. Ed.*, 2016, **55**, 500-513.
113. W. Qian, J. Texter and F. Yan, *Chem. Soc. Rev.*, 2017, **46**, 1124-1159.
114. S.-Y. Zhang, Q. Zhuang, M. Zhang, H. Wang, Z. Gao, J.-K. Sun and J. Yuan, *Chem. Soc. Rev.*, 2020, **49**, 1726-1755.
115. Y.-S. Ye, J. Rick and B.-J. Hwang, *J. Mater. Chem. A*, 2013, **1**, 2719-2743.
116. J. Yuan, D. Mecerreyes and M. Antonietti, *Prog. Polym. Sci.*, 2013, **38**, 1009-1036.
117. V. Ganesan, *Mol. Syst. Des. Eng.*, 2019, **4**, 280-293.
118. Y. Kitazawa, K. Ueno and M. Watanabe, *Chem. Rec.*, 2018, **18**, 391-409.

119. F. Makhlooghiazad, D. Gunzelmann, M. Hilder, D. R. MacFarlane, M. Armand, P. C. Howlett and M. Forsyth, *Adv. Energy Mater.*, 2017, **7**, 1601272.
120. X. Wang, H. Zhu, G. W. Greene, Y. Zhou, M. Yoshizawa-Fujita, Y. Miyachi, M. Armand, M. Forsyth, J. M. Pringle and P. C. Howlett, *Adv. Mater. Technol.*, 2017, **2**, n/a.
121. D. R. MacFarlane and M. Forsyth, *Adv. Mater.*, 2001, **13**, 957-966.
122. K. Romanenko, L. Jin, P. Howlett and M. Forsyth, *Chem. Mater.*, 2016, **28**, 2844-2851.
123. W. Wang, Z. Fang, M. Zhao, Y. Peng, J. Zhang and S. Guan, *Chem. Phys. Lett.*, 2020, **747**, 137335.
124. L. Jin, P. C. Howlett, J. M. Pringle, J. Janikowski, M. Armand, D. R. MacFarlane and M. Forsyth, *Energy Environ. Sci.*, 2014, **7**, 3352-3361.
125. K. Romanenko, L. Jin, L. A. Madsen, J. M. Pringle, L. A. O'Dell and M. Forsyth, *J. Am. Chem. Soc.*, 2014, **136**, 15638-15645.
126. N. Iranipour, D. J. Gunzelmann, A. J. Seeber, J. Vongsvivut, A. F. Hollenkamp, M. Forsyth and P. C. Howlett, *J. Mater. Chem. A*, 2017, **5**, 24909-24919.
127. X. Li, Z. Zhang, S. Li, K. Yang and L. Yang, *J. Mater. Chem. A*, 2017, **5**, 21362-21369.
128. X. Wang, H. Zhu, G. W. Greene, J. Li, N. Iranipour, C. Garnier, J. Fang, M. Armand, M. Forsyth, J. M. Pringle and P. C. Howlett, *J. Mater. Chem. A*, 2016, **4**, 9873-9880.
129. P. C. Howlett, F. Ponzio, J. Fang, T. Lin, L. Jin, N. Iranipour and J. Efthimiadis, *Phys. Chem. Chem. Phys.*, 2013, **15**, 13784-13789.
130. H. Zhu, D. R. MacFarlane, J. M. Pringle and M. Forsyth, *Trends Chem.*, 2019, **1**, 126-140.
131. H. Xue, R. Verma and J. n. M. Shreeve, *J. Fluorine Chem.*, 2006, **127**, 159-176.
132. H. Ohno, *Electrochemical Aspects of Ionic Liquids, 2nd edn.*, John Wiley & Sons Inc., Hoboken, NJ, 2011.
133. K. Matsumoto and R. Hagiwara, *J. Fluorine Chem.*, 2007, **128**, 317-331.
134. G. B. Appetecchi, M. Montanino and S. Passerini, in *Ionic Liquids: Science and Applications*, American Chemical Society, 2012, vol. 1117, ch. 4, pp. 67-128.
135. M. Forsyth, F. Chen, L. A. O'Dell and K. Romanenko, *Solid State Ionics*, 2016, **288**, 160-166.
136. M. Forsyth, G. M. A. Girard, A. Basile, M. Hilder, D. R. MacFarlane, F. Chen and P. C. Howlett, *Electrochim. Acta*, 2016, **220**, 609-617.
137. K. Matsumoto, Y. Okamoto, T. Nohira and R. Hagiwara, *J. Phys. Chem. C*, 2015, **119**, 7648-7655.
138. F. Wu, N. Zhu, Y. Bai, L. Liu, H. Zhou and C. Wu, *ACS Appl. Mater. Interfaces*, 2016, **8**, 21381-21386.
139. N. Wongittharom, T.-C. Lee, C.-H. Wang, Y.-C. Wang and J.-K. Chang, *J. Mater. Chem. A*, 2014, **2**, 5655-5661.
140. K. Matsumoto, R. Taniki, T. Nohira and R. Hagiwara, *J. Electrochem. Soc.*, 2015, **162**, A1409-A1414.
141. K. Matsumoto, T. Hosokawa, T. Nohira, R. Hagiwara, A. Fukunaga, K. Numata, E. Itani, S. Sakai, K. Nitta and S. Inazawa, *J. Power Sources*, 2014, **265**, 36-39.
142. F. Makhlooghiazad, R. Yunis, D. Mecerreyes, M. Armand, P. C. Howlett and M. Forsyth, *Solid State Ionics*, 2017, **312**, 44-52.
143. J. Fuller, R. T. Carlin, H. C. De Long and D. Haworth, *J. Chem. Soc., Chem. Commun.*, 1994, 299-300.
144. J. S. Wilkes and M. J. Zaworotko, *J. Chem. Soc., Chem. Commun.*, 1992, 965-967.
145. A. Noda, K. Hayamizu and M. Watanabe, *J. Phys. Chem. B*, 2001, **105**, 4603-4610.
146. S. Seki, N. Kihira, T. Kobayashi, Y. Kobayashi, Y. Mita, K. Takei, H. Miyashiro and S. Kuwabata, *Electrochemistry*, 2009, **77**, 690-692.
147. H. Matsumoto, H. Sakaebe, K. Tatsumi, M. Kikuta, E. Ishiko and M. Kono, *J. Power Sources*, 2006, **160**, 1308-1313.
148. K. Hayamizu, S. Tsuzuki, S. Seki, K. Fujii, M. Suenaga and Y. Umebayashi, *J. Chem. Phys.*, 2010, **133**, 194505.
149. K. Tsunashima, A. Kawabata, M. Matsumiya, S. Kodama, R. Enomoto, M. Sugiya and Y. Kunugi, *Electrochem. Commun.*, 2011, **13**, 178-181.
150. S. Seki, Y. Ohno, Y. Mita, N. Serizawa, K. Takei and H. Miyashiro, *ECS Electrochem. Lett.*, 2012, **1**, A77-A79.
151. J. Shimada, M. Shimada, T. Sugahara, K. Tsunashima, A. Tani, Y. Tsuchida and M. Matsumiya, *J. Chem. Eng. Data*, 2018, **63**, 3615-3620.
152. A. Best, A. Bhatt and A. Hollenkamp, *J. Electrochem. Soc.*, 2010, **157**, A903-A911.
153. H. Yoon, P. Howlett, A. Best, M. Forsyth and D. MacFarlane, *J. Electrochem. Soc.*, 2013, **160**, A1629-A1637.
154. O. Borodin, W. Gorecki, G. D. Smith and M. Armand, *J. Phys. Chem. B*, 2010, **114**, 6786-6798.
155. A. Budi, A. Basile, G. Opletal, A. F. Hollenkamp, A. S. Best, R. J. Rees, A. I. Bhatt, A. P. O'Mullane and S. P. Russo, *J. Phys. Chem. C*, 2012, **116**, 19789-19797.
156. H. Yang, J. Hwang, Y. Wang, K. Matsumoto and R. Hagiwara, *J. Phys. Chem. C*, 2019, **123**, 22018-22026.
157. M. Ishikawa, T. Sugimoto, M. Kikuta, E. Ishiko and M. Kono, *J. Power Sources*, 2006, **162**, 658-662.
158. K. Matsumoto, T. Hosokawa, T. Nohira, R. Hagiwara, A. Fukunaga, K. Numata, E. Itani, S. Sakai, K. Nitta and S. Inazawa, *J. Power Sources*, 2014, **265**, 36-39.
159. V. Sharova, A. Moretti, T. Diemant, A. Varzi, R. J. Behm and S. Passerini, *J. Power Sources*, 2018, **375**, 43-52.
160. I. A. Shkrob, T. W. Marin, Y. Zhu and D. P. Abraham, *J. Phys. Chem. C*, 2014, **118**, 19661-19671.
161. J. Wang, Y. Yamada, K. Sodeyama, C. H. Chiang, Y. Tateyama and A. Yamada, *Nat. Commun.*, 2016, **7**, 12032.
162. G. Yang, Y. Li, S. Liu, S. Zhang, Z. Wang and L. Chen, *Energy Storage Mater.*, 2019, **23**, 350-357.
163. J. Hwang, K. Matsumoto and R. Hagiwara, *Adv. Energy Mater.*, 2020, **10**, 2001880.
164. J. Sun, L. A. O'Dell, M. Armand, P. C. Howlett and M. Forsyth, *ACS Energy Lett.*, 2021, DOI: 10.1021/acsenergylett.1c00816, 2481-2490.
165. K. Kubota, T. Nohira and R. Hagiwara, *Electrochim. Acta*, 2012, **66**, 320-324.
166. L. Suo, O. Borodin, W. Sun, X. Fan, C. Yang, F. Wang, T. Gao, Z. Ma, M. Schroeder, A. von Cresce, S. M. Russell, M. Armand, A. Angell, K. Xu and C. Wang, *Angew. Chem., Int. Ed.*, 2016, **55**, 7136-7141.
167. J. Hwang, A. N. Sivasengaran, H. Yang, H. Yamamoto, T. Takeuchi, K. Matsumoto and R. Hagiwara, *ACS Appl. Mater. Interfaces*, 2021, **13**, 2538-2546.
168. L. Suo, O. Borodin, T. Gao, M. Olguin, J. Ho, X. Fan, C. Luo, C. Wang and K. Xu, *Science*, 2015, **350**, 938-943.
169. L. Chen, J. Zhang, Q. Li, J. Vatamanu, X. Ji, T. P. Pollard, C. Cui, S. Hou, J. Chen, C. Yang, L. Ma, M. S. Ding, M. Garaga, S. Greenbaum, H.-S. Lee, O. Borodin, K. Xu and C. Wang, *ACS Energy Lett.*, 2020, **5**, 968-974.
170. S. Ko, Y. Yamada and A. Yamada, *Electrochem. Commun.*, 2020, **116**, 106764.

171. T. Mandai, K. Dokko and M. Watanabe, *Chem. Rec.*, 2019, **19**, 708-722.
172. W. A. Henderson, *J. Phys. Chem. B*, 2006, **110**, 13177-13183.
173. T. Mandai, K. Yoshida, S. Tsuzuki, R. Nozawa, H. Masu, K. Ueno, K. Dokko and M. Watanabe, *J. Phys. Chem. B*, 2015, **119**, 1523-1534.
174. W. A. Henderson, F. McKenna, M. A. Khan, N. R. Brooks, V. G. Young and R. Frech, *Chem. Mater.*, 2005, **17**, 2284-2289.
175. S. Menne, J. Pires, M. Anouti and A. Balducci, *Electrochem. Commun.*, 2013, **31**, 39-41.
176. G. Lingua, M. Falco, T. Stettner, C. Gerbaldi and A. Balducci, *J. Power Sources*, 2021, **481**, 228979.
177. A. Basile, M. Hilder, F. Makhlooghiazad, C. Pozo-Gonzalo, D. R. MacFarlane, P. C. Howlett and M. Forsyth, *Adv. Energy Mater.*, 2018, **8**, 1703491.
178. J. P. Hallett and T. Welton, *Chem. Rev.*, 2011, **111**, 3508-3576.
179. M. Petkovic, K. R. Seddon, L. P. N. Rebelo and C. Silva Pereira, *Chem. Soc. Rev.*, 2011, **40**, 1383-1403.
180. D. R. MacFarlane, N. Tachikawa, M. Forsyth, J. M. Pringle, P. C. Howlett, G. D. Elliott, J. H. Davis, M. Watanabe, P. Simon and C. A. Angell, *Energy Environ. Sci.*, 2014, **7**, 232-250.
181. N. V. Plechkova and K. R. Seddon, *Chem. Soc. Rev.*, 2008, **37**, 123-150.
182. C. D. Hubbard, P. Illner and R. van Eldik, *Chem. Soc. Rev.*, 2011, **40**, 272-290.
183. A. Basile, A. I. Bhatt and A. P. O'Mullane, *Nat. Commun.*, 2016, **7**, 11794.
184. H. Yoon, G. H. Lane, Y. Shekibi, P. C. Howlett, M. Forsyth, A. S. Best and D. R. MacFarlane, *Energy Environ. Sci.*, 2013, **6**, 979-986.
185. H. Sano, M. Kitta and H. Matsumoto, *J. Electrochem. Soc.*, 2016, **163**, D3076-D3079.
186. F. Mizuno, T. S. Arthur and K. Takechi, *ACS Energy Lett.*, 2016, **1**, 542-547.
187. J. Hwang, H. Okada, R. Haraguchi, S. Tawa, K. Matsumoto and R. Hagiwara, *J. Power Sources*, 2020, **453**, 227911.
188. S. Wenzel, T. Leichtweiss, D. Krüger, J. Sann and J. Janek, *Solid State Ionics*, 2015, **278**, 98-105.
189. A. Vioux and B. Coasne, *Adv. Energy Mater.*, 2017, **7**, 1700883.
190. J. Le Bideau, L. Viau and A. Vioux, *Chem. Soc. Rev.*, 2011, **40**, 907-925.
191. N. Chen, H. Zhang, L. Li, R. Chen and S. Guo, *Adv. Energy Mater.*, 2018, **8**, 1702675.
192. A. K. Tripathi, *Mater. Today Energy*, 2021, **20**, 100643.
193. S. Dai, Y. H. Ju, H. J. Gao, J. S. Lin, S. J. Pennycook and C. E. Barnes, *Chem. Commun.*, 2000, 243-244.
194. N. Kimizuka and T. Nakashima, *Langmuir*, 2001, **17**, 6759-6761.
195. C. P. Mehnert, R. A. Cook, N. C. Dispenziere and M. Afeworki, *J. Am. Chem. Soc.*, 2002, **124**, 12932-12933.
196. F. Wu, G. Tan, R. Chen, L. Li, J. Xiang and Y. Zheng, *Adv. Mater.*, 2011, **23**, 5081-5085.
197. X. Chen, B. Put, A. Sagara, K. Gandrud, M. Murata, J. A. Steele, H. Yabe, T. Hantschel, M. Roeffaers, M. Tomiyama, H. Arase, Y. Kaneko, M. Shimada, M. Mees and P. M. Vereecken, *Sci. Adv.*, 2020, **6**, eaav3400.
198. A. Sagara, X. Chen, K. B. Gandrud, M. Murata, M. Mees, Y. Kaneko, H. Arase and P. M. Vereecken, *J. Electrochem. Soc.*, 2020, **167**, 070549.
199. Z. Wang, R. Tan, H. Wang, L. Yang, J. Hu, H. Chen and F. Pan, *Adv. Mater.*, 2018, **30**, 1704436.
200. F. Wu, N. Chen, R. Chen, Q. Zhu, J. Qian and L. Li, *Chem. Mater.*, 2016, **28**, 848-856.
201. J. Tong, S. Wu, N. von Solms, X. Liang, F. Huo, Q. Zhou, H. He and S. Zhang, *Front. Chem.*, 2020, **7**.
202. K. Fujie, R. Ikeda, K. Otsubo, T. Yamada and H. Kitagawa, *Chem. Mater.*, 2015, **27**, 7355-7361.
203. K. Kalaga, M.-T. F. Rodrigues, H. Gullapalli, G. Babu, L. M. R. Arava and P. M. Ajayan, *ACS Appl. Mater. Interfaces*, 2015, **7**, 25777-25783.
204. G. Tan, F. Wu, C. Zhan, J. Wang, D. Mu, J. Lu and K. Amine, *Nano Lett.*, 2016, **16**, 1960-1968.
205. T. Yuuki, Y. Konosu, M. Ashizawa, T. Iwahashi, Y. Ouchi, Y. Tominaga, R. Ooyabu, H. Matsumoto and H. Matsumoto, *ACS Omega*, 2017, **2**, 835-841.
206. J.-K. Kim, J. Scheers, T. J. Park and Y. Kim, *ChemSusChem*, 2015, **8**, 636-641.
207. W. J. Hyun, A. C. M. de Moraes, J.-M. Lim, J. R. Downing, K.-Y. Park, M. T. Z. Tan and M. C. Hersam, *ACS Nano*, 2019, **13**, 9664-9672.
208. Y. Lu, K. Korf, Y. Kambe, Z. Tu and L. A. Archer, *Angew. Chem., Int. Ed.*, 2014, **53**, 488-492.
209. P. Chiochan, X. Yu, M. Sawangphruk and A. Manthiram, *Adv. Energy Mater.*, 2020, **10**, 2001285.
210. X. Liu, J.-Q. Huang, Q. Zhang and L. Mai, *Adv. Mater.*, 2017, **29**, 1601759.
211. J. Zhang, Y. Bai, X.-G. Sun, Y. Li, B. Guo, J. Chen, G. M. Veith, D. K. Hensley, M. P. Paranthaman, J. B. Goodenough and S. Dai, *Nano Lett.*, 2015, **15**, 3398-3402.
212. A. Singh, R. Vedarajan and N. Matsumi, *J. Electrochem. Soc.*, 2017, **164**, H5169-H5174.
213. P. C. Marr and A. C. Marr, *Green Chem.*, 2016, **18**, 105-128.
214. F. Borghi and A. Podestà, *Adv. Phys-X*, 2020, **5**, 1736949.
215. D. S. Ashby, R. H. DeBlock, C. S. Choi, W. Sugimoto and B. Dunn, *ACS Appl. Mater. Interfaces*, 2019, **11**, 12088-12097.
216. B. P. Thapaliya, C.-L. Do-Thanh, C. J. Jafta, R. Tao, H. Lyu, A. Y. Borisevich, S.-z. Yang, X.-G. Sun and S. Dai, *Batter. Supercaps*, 2019, **2**, 985-991.
217. A. Guyomard-Lack, B. Said, N. Dupré, A. Galarneau and J. Le Bideau, *New J. Chem.*, 2016, **40**, 4269-4276.
218. X. Li, S. Li, Z. Zhang, J. Huang, L. Yang and S.-i. Hirano, *J. Mater. Chem. A*, 2016, **4**, 13822-13829.
219. F. Wu, N. Chen, R. Chen, L. Wang and L. Li, *Nano Energy*, 2017, **31**, 9-18.
220. Y. Lu, S. K. Das, S. S. Moganty and L. A. Archer, *Adv. Mater.*, 2012, **24**, 4430-4435.
221. T. Matsuo, Y. Gambe, Y. Sun and I. Honma, *Sci. Rep.*, 2014, **4**, 6084.
222. Z. Wen, Y. Li, Z. Zhao, W. Qu, N. Chen, Y. Xing, Y. Ma, L. Li, F. Wu and R. Chen, *J. Mater. Chem. A*, 2020, **8**, 7280-7287.
223. R. Chen, W. Qu, J. Qian, N. Chen, Y. Dai, C. Guo, Y. Huang, L. Li and F. Wu, *J. Mater. Chem. A*, 2017, **5**, 24677-24685.
224. W. Qu, M. Yan, R. Luo, J. Qian, Z. Wen, N. Chen, L. Li, F. Wu and R. Chen, *J. Power Sources*, 2021, **484**, 229195.
225. N. Chen, Y. Xing, L. Wang, F. Liu, L. Li, R. Chen, F. Wu and S. Guo, *Nano Energy*, 2018, **47**, 35-42.
226. Y. Yoshida and H. Kitagawa, *ACS Sustain. Chem. Eng.*, 2019, **7**, 70-81.
227. F. P. Kinik, A. Uzun and S. Keskin, *ChemSusChem*, 2017, **10**, 2842-2863.
228. T. Tsuda, C.-Y. Chen and C. L. Hussey, in *Ionic Liquid Devices*, The Royal Society of Chemistry, 2018, DOI:

10.1039/9781788011839-00001, pp. 1-29.
229. J. H. Lee, A. S. Lee, S. M. Hong, S. S. Hwang and C. M. Koo, *Polymer*, 2017, **117**, 160-166.
230. M.-T. F. Rodrigues, G. Babu, H. Gullapalli, K. Kalaga, F. N. Sayed, K. Kato, J. Joyner and P. M. Ajayan, *Nat. Energy*, 2017, **2**, 17108.
231. S. Horike, D. Umeyama and S. Kitagawa, *Accounts Chem Res*, 2013, **46**, 2376-2384.
232. Y. He, Y. Qiao, Z. Chang and H. Zhou, *Energy Environ. Sci.*, 2019, **12**, 2327-2344.
233. R. Zhao, Y. Wu, Z. Liang, L. Gao, W. Xia, Y. Zhao and R. Zou, *Energy Environ. Sci.*, 2020, **13**, 2386-2403.
234. L. Feng, K.-Y. Wang, G. S. Day and H.-C. Zhou, *Chem. Soc. Rev.*, 2019, **48**, 4823-4853.
235. M. Kalaj, K. C. Bentz, S. Ayala, J. M. Palomba, K. S. Barcus, Y. Katayama and S. M. Cohen, *Chem. Rev.*, 2020, **120**, 8267-8302.
236. H. Furukawa, K. E. Cordova, M. O'Keeffe and O. M. Yaghi, *Science*, 2013, **341**, 1230444.
237. M. Ue, A. Murakami and S. Nakamura, *J. Electrochem. Soc.*, 2002, **149**, A1385.
238. C. Largeot, C. Portet, J. Chmiola, P. L. Taberna, Y. Gogotsi and P. Simon, *J. Am. Chem. Soc.*, 2008, **130**, 2730-2731.
239. M. Sun, T. Liu, Y. Yuan, M. Ling, N. Xu, Y. Liu, L. Yan, H. Li, C. Liu, Y. Lu, Y. Shi, Y. He, Y. Guo, X. Tao, C. Liang and J. Lu, *ACS Energy Lett.*, 2021, **6**, 451-458.
240. S. S. Park, Y. Tulchinsky and M. Dincă, *J. Am. Chem. Soc.*, 2017, **139**, 13260-13263.
241. E. M. Miner, S. S. Park and M. Dincă, *J. Am. Chem. Soc.*, 2019, **141**, 4422-4427.
242. Y. Xiao, Y. Wang, S.-H. Bo, J. C. Kim, L. J. Miara and G. Ceder, *Nat. Rev. Mater.*, 2020, **5**, 105-126.
243. J. Timmermans, *J. Phys. Chem. Solids*, 1961, **18**, 1-8.
244. S. Das, A. Mondal and C. M. Reddy, *Chem. Soc. Rev.*, 2020, **49**, 8878-8896.
245. R. Aronsson, B. Jansson, H. Knape, A. Lundén, L. Nilsson, C.-A. SjÖblom and L. Torell, *J. Phys. Colloq.*, 1980, **41**, C6-35-C36-37.
246. J. M. Pringle, P. C. Howlett, D. R. MacFarlane and M. Forsyth, *J. Mater. Chem.*, 2010, **20**, 2056-2062.
247. J. M. Pringle, *Phys. Chem. Chem. Phys.*, 2013, **15**, 1339-1351.
248. K. Goossens, L. Rakers, B. Heinrich, G. Ahumada, T. Ichikawa, B. Donnio, T. J. Shin, C. W. Bielawski and F. Glorius, *Chem. Mater.*, 2019, **31**, 9593-9603.
249. C. B. Park and B. J. Sung, *J. Phys. Chem. C*, 2020, **124**, 6894-6904.
250. J. Golding, N. Hamid, D. R. MacFarlane, M. Forsyth, C. Forsyth, C. Collins and J. Huang, *Chem. Mater.*, 2001, **13**, 558-564.
251. S. Forsyth, J. Golding, D. R. MacFarlane and M. Forsyth, *Electrochim. Acta*, 2001, **46**, 1753-1757.
252. D. R. MacFarlane, P. Meakin, J. Sun, N. Amini and M. Forsyth, *J. Phys. Chem. C*, 1999, **103**, 4164-4170.
253. H. Zhu, F. Chen, L. Jin, L. A. O'Dell and M. Forsyth, *ChemPhysChem*, 2014, **15**, 3720-3724.
254. M. Volel, P.-J. Alarco, Y. Abu-Lebdeh and M. Armand, *ChemPhysChem*, 2004, **5**, 1027-1033.
255. Z.-B. Zhou and H. Matsumoto, *Electrochem. Commun.*, 2007, **9**, 1017-1022.
256. W. A. Henderson, M. Herstedt, V. G. Young, Jr., S. Passerini, H. C. De Long and P. C. Trulove, *Inorg. Chem.*, 2006, **45**, 1412-1414.
257. D. R. MacFarlane, P. Meakin, N. Amini and M. Forsyth, *J. Phys.: Condens. Matter*, 2001, **13**, 8257-8267.
258. W. A. Henderson, V. G. Young, S. Passerini, P. C. Trulove and H. C. De Long, *Chem. Mater.*, 2006, **18**, 934-938.
259. G. Annat, J. Adebahr, I. R. McKinnon, D. R. MacFarlane and M. Forsyth, *Solid State Ionics*, 2007, **178**, 1065-1071.
260. S. J. Pas, J. M. Pringle, M. Forsyth and D. R. MacFarlane, *Phys. Chem. Chem. Phys.*, 2004, **6**, 3721-3725.
261. A. J. Seeber, M. Forsyth, C. M. Forsyth, S. A. Forsyth, G. Annat and D. R. MacFarlane, *Phys. Chem. Chem. Phys.*, 2003, **5**, 2692-2698.
262. J. Adebahr, M. Grirnsley, N. M. Rocher, D. R. MacFarlane and M. Forsyth, *Solid State Ionics*, 2008, **178**, 1798-1803.
263. J. Adebahr, M. Forsyth and D. R. MacFarlane, *Electrochim. Acta*, 2005, **50**, 3853-3858.
264. J. Sun, D. R. MacFarlane and M. Forsyth, *Solid State Ionics*, 2002, **148**, 145-151.
265. Z. B. Zhou, H. Matsumoto and K. Tatsumi, *Chem. Eur. J*, 2006, **12**, 2196-2212.
266. M. Yoshizawa-Fujita, H. Yamada, S. Yamaguchi, H. Zhu, M. Forsyth, Y. Takeoka and M. Rikukawa, *Batter. Supercaps*, 2020, **3**, 884-891.
267. S. Yamaguchi, H. Yamada, Y. Takeoka, M. Rikukawa and M. Yoshizawa-Fujita, *New J. Chem.*, 2019, **43**, 4008-4012.
268. R. Yunis, T. W. Newbegin, A. F. Hollenkamp and J. M. Pringle, *Mater. Chem. Front.*, 2018, **2**, 1207-1214.
269. C. Shi, S. Li, W. Zhang, L. Qiu and F. Yan, *J. Mater. Chem. A*, 2013, **1**, 13956-13962.
270. T. Ruther, J. Huang and A. F. Hollenkamp, *Chem. Commun.*, 2007, 5226-5228.
271. J. M. Pringle, J. Adebahr, D. R. MacFarlane and M. Forsyth, *Phys. Chem. Chem. Phys.*, 2010, **12**, 7234-7240.
272. M. Yoshizawa-Fujita, E. Kishi, M. Suematsu, T. Takekawa and M. Rikukawa, *Chem. Lett.*, 2014, **43**, 1909-1911.
273. M. Moriya, T. Watanabe, W. Sakamoto and T. Yogo, *RSC Adv.*, 2012, **2**, 8502-8507.
274. R. Yunis, A. F. Hollenkamp, C. Forsyth, C. M. Doherty, D. Al-Masri and J. M. Pringle, *Phys. Chem. Chem. Phys.*, 2019, **21**, 12288-12300.
275. R. Yunis, D. Al-Masri, A. F. Hollenkamp, C. M. Doherty, H. Zhu and J. M. Pringle, *J. Electrochem. Soc.*, 2020, **167**, 070529.
276. K. Matsumoto, R. Nonaka, Y. Wang, G. Veryasov and R. Hagiwara, *Phys. Chem. Chem. Phys.*, 2017, **19**, 2053-2059.
277. K. Matsumoto, U. Harinaga, R. Tanaka, A. Koyama, R. Hagiwara and K. Tsunashima, *Phys. Chem. Chem. Phys.*, 2014, **16**, 23616-23626.
278. O. Hiroshi, I. Shin'ichi, I. Ryuichi and I. Hiroyuki, *Bull. Chem. Soc. Jpn.*, 1999, **72**, 2049-2054.
279. T. Shimizu, S. Tanaka, N. Onoda-Yamamuro, S. i. Ishimaru and R. Ikeda, *J. Chem. Soc., Faraday Trans.*, 1997, **93**, 321-326.
280. L. Jin, K. M. Nairn, C. D. Ling, H. Zhu, L. A. O'Dell, J. Li, F. Chen, A. F. Pavan, L. A. Madsen, P. C. Howlett, D. R. MacFarlane, M. Forsyth and J. M. Pringle, *J. Phys. Chem. B*, 2017, **121**, 5439-5446.
281. W. A. Henderson, M. Herstedt, V. G. Young, S. Passerini, H. C. De Long and P. C. Trulove, *Inorg. Chem.*, 2006, **45**, 1412-1414.
282. A. R. Choudhury, N. Winterton, A. Steiner, A. I. Cooper and K. A. Johnson, *J. Am. Chem. Soc.*, 2005, **127**, 16792-16793.
283. L. Jin, K. M. Nairn, C. M. Forsyth, A. J. Seeber, D. R. MacFarlane, P. C. Howlett, M. Forsyth and J. M. Pringle, *J. Am. Chem. Soc.*, 2012, **134**, 9688-9697.
284. F. Chen, L. Jin, S. W. d. Leeuw, J. M. Pringle and M. Forsyth, *J. Chem. Phys.*, 2013, **138**, 244503.
285. A. Mondal, B. Bhattacharya, S. Das, S. Bhunia, R.

Chowdhury, S. Dey and C. M. Reddy, *Angew. Chem., Int. Ed.*, 2020, **59**, 10971-10980.
286. J. Harada, T. Shimojo, H. Oyamaguchi, H. Hasegawa, Y. Takahashi, K. Satomi, Y. Suzuki, J. Kawamata and T. Inabe, *Nat. Chem.*, 2016, **8**, 946-952.
287. K. Yang, Z. Zhang, Z. Liao, L. Yang and S.-i. Hirano, *Chemistryselect*, 2018, **3**, 12595-12599.
288. F. Ramos, M. Forsyth and J. M. Pringle, *ChemSusChem*, 2020, **13**, 5740-5748.
289. L. Jin, P. Howlett, J. Efthimiadis, M. Kar, D. MacFarlane and M. Forsyth, *J. Mater. Chem.*, 2011, **21**, 10171-10178.
290. S. Seki, Y. Umebayashi, S. Tsuzuki, K. Hayamizu, Y. Kobayashi, Y. Ohno, T. Kobayashi, Y. Mita, H. Miyashiro, N. Terada and S. Ishiguro, *Chem. Commun.*, 2008, DOI: 10.1039/b809309a, 5541-5543.
291. H. Zhu and M. Forsyth, *J. Phys. Chem. Lett.*, 2020, **11**, 510-515.
292. J. H. Huang, A. Hill, M. Forsyth, D. MacFarlane and A. Hollenkamp, *Solid State Ionics*, 2006, **177**, 2569-2573.
293. S. J. Pas, J. Huang, M. Forsyth, D. R. MacFarlane and A. J. Hill, *J. Chem. Phys.*, 2005, **122**, 064704.
294. F. Chen, S. W. de Leeuw and M. Forsyth, *J. Phys. Chem. Lett.*, 2013, **4**, 4085-4089.
295. K. Romanenko, J. M. Pringle, L. A. O'Dell and M. Forsyth, *Phys. Chem. Chem. Phys.*, 2015, **17**, 18991-19000.
296. B. E. Kidd, M. D. Lingwood, M. Lee, H. W. Gibson and L. A. Madsen, *J. Phys. Chem. C*, 2014, **118**, 2176-2185.
297. I. Popov, K. Biernacka, H. Zhu, F. Nti, L. Porcarelli, X. Wang, A. Khamzin, C. Gainaru, M. Forsyth and A. P. Sokolov, *J. Phys. Chem. C*, 2020, **124**, 17889-17896.
298. M. Matsuki, T. Yamada, N. Yasuda, S. Dekura, H. Kitagawa and N. Kimizuka, *J. Am. Chem. Soc.*, 2018, **140**, 291-297.
299. M. Matsuki, T. Yamada, S. Dekura, H. Kitagawa and N. Kimizuka, *Chem. Lett.*, 2018, **47**, 497-499.
300. H. Yamada, Y. Miyachi, Y. Takeoka, M. Rikukawa and M. Yoshizawa-Fujita, *Electrochim. Acta*, 2019, **303**, 293-298.
301. X.-y. Zhao, J.-l. Wang, H. Luo, H.-r. Yao, C.-y. Ouyang and L.-z. Zhang, *J. Zhejiang Univ., Sci., A*, 2016, **17**, 155-162.
302. J. Adebahr, A. J. Seeber, D. R. MacFarlane and M. Forsyth, *J. Phys. Chem. C*, 2005, **109**, 20087-20092.
303. D. R. MacFarlane, J. Huang and M. Forsyth, *Nature*, 1999, **402**, 792-794.
304. Y. Abu-Lebdeh, A. Abouimrane, P.-J. Alarco and M. Armand, *J. Power Sources*, 2006, **154**, 255-261.
305. K. Biernacka, D. Al-Masri, R. Yunis, H. Zhu, A. F. Hollenkamp and J. M. Pringle, *Electrochim. Acta*, 2020, **357**, 136863.
306. K. Yang, Z. Liao, Z. Zhang, L. Yang and S.-i. Hirano, *Mater. Lett.*, 2019, **236**, 554-557.
307. W. A. Henderson, D. M. Seo, Q. Zhou, P. D. Boyle, J. H. Shin, H. C. De Long, P. C. Trulove and S. Passerini, *Adv. Energy Mater.*, 2012, **2**, 1343-1350.
308. S. Murugesan, O. A. Quintero, B. P. Chou, P. Xiao, K. Park, J. W. Hall, R. A. Jones, G. Henkelman, J. B. Goodenough and K. J. Stevenson, *J. Mater. Chem. A*, 2014, **2**, 2194-2201.
309. F. Chen, J. M. Pringle and M. Forsyth, *Chem. Mater.*, 2015, **27**, 2666-2672.
310. L. Jin, S. de Leeuw, M. V. Koudriachova, J. M. Pringle, P. C. Howlett, F. Chen and M. Forsyth, *Phys. Chem. Chem. Phys.*, 2013, **15**, 19570-19574.
311. E. I. Cooper and C. A. Angell, *Solid State Ionics*, 1986, **18-19**, 570-576.
312. J. Efthimiadis, G. J. Annat, J. Efthimiadis, M. Forsyth and D. R. MacFarlane, *Phys. Chem. Chem. Phys.*, 2003, **5**, 5558-5564.
313. Y. Abu-Lebdeh, P.-J. Alarco and M. Armand, *Angew. Chem., Int. Ed.*, 2003, **42**, 4499-4501.
314. P.-J. Alarco, Y. Abu-Lebdeh and M. Armand, *Solid State Ionics*, 2004, **175**, 717-720.
315. Y. Shekibi, T. Ruther, J. Huang and A. F. Hollenkamp, *Phys. Chem. Chem. Phys.*, 2012, **14**, 4597-4604.
316. P. C. Howlett, Y. Shekibi, D. R. MacFarlane and M. Forsyth, *Adv Eng Mater*, 2009, **11**, 1044-1048.
317. P. C. Howlett, J. Sunarso, Y. Shekibi, E. Wasser, L. Jin, D. R. MacFarlane and M. Forsyth, *Solid State Ionics*, 2011, **204-205**, 73-79.
318. J. Sunarso, Y. Shekibi, J. Efthimiadis, L. Y. Jin, J. M. Pringle, A. F. Hollenkamp, D. R. MacFarlane, M. Forsyth and P. C. Howlett, *J. Solid State Electrochem.*, 2012, **16**, 1841-1848.
319. L. Suo, Y.-S. Hu, H. Li, M. Armand and L. Chen, *Nat. Commun.*, 2013, **4**, 1481.
320. C. A. Angell, C. Liu and E. Sanchez, *Nature*, 1993, **362**, 137-139.
321. D. Al-Masri, R. Yunis, H. Zhu, L. Jin, P. Bruce, A. F. Hollenkamp and J. M. Pringle, *J. Mater. Chem. A*, 2019, **7**, 25389-25398.
322. D. Al-Masri, R. Yunis, A. F. Hollenkamp and J. M. Pringle, *Chem. Commun.*, 2018, **54**, 3660-3663.
323. M. Forsyth, T. Chimdi, A. Seeber, D. Gunzelmann and P. C. Howlett, *J. Mater. Chem. A*, 2014, **2**, 3993-4003.
324. T. Chimdi, D. Gunzelmann, J. Vongsvivut and M. Forsyth, *Solid State Ionics*, 2015, **272**, 74-83.
325. F. Makhlooghiazad, P. C. Howlett, X. Wang, M. Hilder, D. R. MacFarlane, M. Armand and M. Forsyth, *J. Mater. Chem. A*, 2017, **5**, 5770-5780.
326. F. Makhlooghiazad, J. Guazzagaloppa, L. A. O'Dell, R. Yunis, A. Basile, P. C. Howlett and M. Forsyth, *Phys. Chem. Chem. Phys.*, 2018, **20**, 4721-4731.
327. M. Forsyth, H. Yoon, F. Chen, H. Zhu, D. R. MacFarlane, M. Armand and P. C. Howlett, *J. Phys. Chem. C*, 2016, **120**, 4276-4286.
328. C.-Y. Chen, T. Kiko, T. Hosokawa, K. Matsumoto, T. Nohira and R. Hagiwara, *J. Power Sources*, 2016, **332**, 51-59.
329. J. Hwang, K. Matsumoto and R. Hagiwara, *Adv. Sustainable Syst.*, 2018, **2**, 1700171.
330. C. V. Manohar, T. C. Mendes, M. Kar, D. wang, C. Xiao, M. Forsyth, S. Mitra and D. R. MacFarlane, *Chem. Commun.*, 2018, **54**, 3500-3503.
331. J. Hwang, K. Matsumoto and R. Hagiwara, *J. Phys. Chem. C*, 2018, **122**, 26857-26864.
332. J. Efthimiadis, G. Annat, J. Efthimiadis, D. R. MacFarlane and M. Forsyth, *Solid State Ionics*, 2006, **177**, 95-104.
333. F. Nti, L. Porcarelli, G. W. Greene, H. Zhu, F. Makhlooghiazad, D. Mecerreyes, P. C. Howlett, M. Forsyth and X. Wang, *J. Mater. Chem. A*, 2020, **8**, 5350-5362.
334. N. Iranipour, D. J. Gunzelmann, A. Seeber, J. Vongsvivut, C. Doherty, F. Ponzio, L. A. O'Dell, A. F. Hollenkamp, M. Forsyth and P. C. Howlett, *J. Mater. Chem. A*, 2015, **3**, 6038-6052.
335. Y. Zhou, X. Wang, H. Zhu, M. Armand, M. Forsyth, G. W. Greene, J. M. Pringle and P. C. Howlett, *Phys. Chem. Chem. Phys.*, 2017, **19**, 2225-2234.
336. Y. Zhou, X. Wang, H. Zhu, M. Yoshizawa-Fujita, Y. Miyachi, M. Armand, M. Forsyth, G. W. Greene, J. M. Pringle and P. C. Howlett, *ChemSusChem*, 2017, **10**, 3135-3145.
337. K. Matsumoto, E. Nishiwaki, T. Hosokawa, S. Tawa, T. Nohira and R. Hagiwara, *J. Phys. Chem. C*, 2017, **121**, 9209-9219.

338. Y. Zhou, X. Wang, H. Zhu, M. Armand, M. Forsyth, G. W. Greene, J. M. Pringle and P. C. Howlett, *Energy Storage Mater.*, 2018, **15**, 407-414.
339. S. Li, K. Yang, Z. Zhang, L. Yang and S.-i. Hirano, *Ind. Eng. Chem. Res.*, 2018, **57**, 13608-13614.
340. W. Wang, Z. Fang, M. Zhao, Y. Peng, J. Zhang and S. Guan, *Chem Phys Lett*, 2020, **747**, 137335.
341. Z. Liao, J. Huang, W. Chen, N. Saito, Z. Zhang, L. Yang and S.-i. Hirano, *Energy Storage Mater.*, 2020, **33**, 442-451.
342. G. W. Greene, F. Ponzio, N. Iranipour, H. Zhu, A. Seeber, M. Forsyth and P. C. Howlett, *Electrochim. Acta*, 2015, **175**, 214-223.
343. Y. Inaguma, C. Liquan, M. Itoh, T. Nakamura, T. Uchida, H. Ikuta and M. Wakihara, *Solid State Commun.*, 1993, **86**, 689-693.
344. J. Fu, *Solid State Ionics*, 1997, **104**, 191-194.
345. J. Fu, *Solid State Ionics*, 1997, **96**, 195-200.
346. K. Yamamoto, S. Yang, M. Takahashi, K. Ohara, T. Uchiyama, T. Watanabe, A. Sakuda, A. Hayashi, M. Tatsumisago, H. Muto, A. Matsuda and Y. Uchimoto, *ACS Appl. Energy Mater.*, 2021, **4**, 2275-2281.
347. Y. Li, C.-A. Wang, H. Xie, J. Cheng and J. B. Goodenough, *Electrochem. Commun.*, 2011, **13**, 1289-1292.
348. D. Ruzmetov, V. P. Oleshko, P. M. Haney, H. J. Lezec, K. Karki, K. H. Baloch, A. K. Agrawal, A. V. Davydov, S. Krylyuk, Y. Liu, J. Huang, M. Tanase, J. Cumings and A. A. Talin, *Nano Lett.*, 2012, **12**, 505-511.
349. Y. Kato, S. Hori, T. Saito, K. Suzuki, M. Hirayama, A. Mitsui, M. Yonemura, H. Iba and R. Kanno, *Nat. Energy*, 2016, **1**, 16030.
350. F. Makhlooghiazad, M. Sharma, Z. Zhang, L. F. Nazar, F. Makhlooghiazad, P. C. Howlett and M. Forsyth, *J Phys Chem Lett*, 2020, **11**, 2092-2100.

Table 1 Transport properties and electrochemical performance of selected solid-state and pseudo-solid-state electrolytes prepared with ILs.[a]

Group	Ionic liquid	Host material	σ / mS cm^{-1}	t_{Li+}	Battery configuration		Average voltage / V	Reversible capacity / mAh g^{-1}	Characteristics	Ref
					Cathode	Anode				
Solid-state	--	$Li_{0.34}La_{0.51}TiO_{2.94}$	0.02@25 ˚C							343
Solid-state	--	$LiGe_2(PO_4)_3$	0.1@25 ˚C							344
Solid-state	--	Li_2O-Al_2O_3-P_2O_5	1.3@25 ˚C							345
Solid-state	--	$La_7La_3Zr_2O_{12}$	0.3@25 ˚C							21
Solid-state	--	$Li_{10}GeP_2S_{12}$	12@25 ˚C		$LiCoO_2$	Li	--	120	Battery test at 25 ˚C	22
Solid-state	--	Li_3PS_4	0.5@25 ˚C							346
Solid-state	--	$Li_6La_3ZrTaO_{12}$	0.3@25 ˚C							347
Hybrid solid-state	Li[FSA]-G4	Al-LLZO	0.1@25 ˚C		$LiCoO_2$	Li	--	110, 139	Battery test at 30 and 60 ˚C	41
Hybrid solid-state	Li[TFSA]-G4	PEO-LLZO	0.1@25 ˚C		NCM622	Li		150	Battery test at 25 ˚C	53
Hybrid solid-state	$[C_2C_1im][BF_4]$	$La_{2/3-x}Li_{3x}O_3$	--	--	--	--	--	--	E_a (interfacial Li^+ transfer) = 25 kJ mol–1	50
Hybrid solid-state	$[C_6C_1im][BF_4]$	$La_{2/3-x}Li_{3x}O_3$	--	--	--	--	--	--	E_a (interfacial Li^+ transfer) = 47 kJ mol–1	50
Hybrid solid-state	$[C_2C_1im][BETA]$	$La_{2/3-x}Li_{3x}O_3$	--	--	--	--	--	--	E_a (interfacial Li^+ transfer) = 57 kJ mol–1	50
Hybrid solid-state	$[C_2C_1im][TFSA]$	$La_{2/3-x}Li_{3x}O_3$	--	--	--	--	--	--	E_a (interfacial Li^+ transfer) = 62 kJ mol–1	50
Hybrid solid-state	Li[TFSA]–$[C_4C_1pyrr][TFSA]$	$Li_{6.5}La_{2.5}Ba_{0.5}ZrNbO_{12}$	--	--	S	Li		1360	Battery test at 25 ˚C	37
Hybrid solid-state	Li[TFSA]-$[C_3C_1pyrr][TFSA]$	$Li_{10}GeP_2S_{12}$	--		$LiFePO_4$	Li	3.5	144	IL used for SEI formation on IL side Battery test at 25 ˚C	55
Hybrid solid-state	Li[TFSA]-$[C_4C_1pyrr][FSA]$	LLZO	--		$LiFePO_4$	Li	3.5	145	Interfacial resistance reduced from 2440 to 145Ω cm^2 with IL Battery test at 25 ˚C	38
Hybrid solid-state	$[C_3C_1pyrr][FSA]$	$Na_3Zr_2Si_2PO_{12}$			$Na_3V_2(PO_4)_3$	Na	3.4	115	IL as the wetting agent Battery test at 25 ˚C Rate and cycle performance improved	30
Hybrid solid-state	$[C_3C_1pyrr][FSA]$	$Na_{3+x}La_xZr_{2-x}Si_2PO_{12}$			$Na_3V_2(PO_4)_3$	Na	3.4	116	IL used as the wetting agent Battery test at 25 ˚C Rate and cycle performance improved	30
Hybrid solid-state	Li[TFSA]-G3	$Li_{10}GeP_2S_{12}$			Li	$Li_4Ti_5O_{12}$		160	Solvate IL used for interface modification Battery test at room temperature	42
Solid-state	--	$Na_3Si_2Y_{0.16}Zr_{1.84}PO_{12}$	1.1×10^{-3}@20 ˚C							46
Hybrid solid-state	$[C_4C_1pyrr][TFSA]$	$Na_3Si_2Y_{0.16}Zr_{1.84}PO_{12}$	0.06@20 ˚C						IL:solid-state electrolyte = 5:95 wt%	46

Hybrid solid-state	Na[TFSA]-[C_4C_1pyrr][TFSA]	$Na_3Si_2Y_{0.16}Zr_{1.84}PO_{12}$	0.36@20 ˚C					IL:solid-state electrolyte = 10:90 wt%	46
Hybrid solid-state	Li[TFSA]-[C_4C_1pyrr][TFSA]	$Li_{6.4}La_3Zr_{1.4}Ta_{0.6}O_{12}$	1.71@60 ˚C	0.56	O_2	Li	Fixed capacity	Battery test at 60 ˚C	47
Hybrid solid-state	Li[TFSA]–[C_3C_1pyrr][FSA]	LISICON			Li	Graphite	134 285 320	IL used as the wetting agent Battery test at 25, 50, and 120 ˚C	36
Hybrid solid-state	Li[TFSA]-[C_4C_1pyrr][TFSA]	$Li_7La_3Zr_2O_{12}$	0.4@25 ˚C		$LiCO_2$	Li	140	Battery test at 25 ˚C	39
Hybrid solid-state	[C_2C_1im][FSA]	$Li_{6.5}Mg_{0.05}La_3Zr_{1.6}Ta_{0.4}O_1$-PEO	0.1@40 ˚C						52
Hybrid solid-state	[AMim][TFSA]	$Li_{6.4}La_3Ta_{0.6}Zr_{1.4}O_{12}$	2.5@20 ˚C		S	Li	340	Battery test at 20 ˚C	57
Hybrid solid-state	Li[TFSA]-[C_2C_1im][TFSA]	$Li_7La_3Zr_2O_{12}$-PVDF-HFP	6.5@room temp.		$LiFePO_4$	$Li_4Ti_5O_{12}$	103	Full cell test at room temp.	40
Hybrid solid-state	Li[TFSA]-G3	Li_3PS_4	~1@20 ˚C				144	Battery test at 30 ˚C	56
Hybrid solid-state	Li[TFSA]-G3	$Li_{10}GeP_2S_{12}$	~5@20 ˚C		$LiFePO_4$	Li-In	144		
Ionogel	Li[FSA]–[C_2C_1im][FSA]	Silica	6.2@25 ˚C	--	$LiFePO_4$	Li	3.5 150	Battery test at 30 ˚C	198
Ionogel	Li[TFSA]–[C_4C_1pyrr][TFSA]	Silica with a chemisorbed water layer	5.4@25 ˚C[a]	--	$LiFePO_4$	Li	3.5 140	Battery test at 25 ˚C T_d > 320 ˚C 200% higher σ than the pure IL	197
Ionogel	Li[TFSA]–[C_4C_1im][TFSA]	Silica	3.6@25 ˚C	--	$LiNi_{1/3}Co_{1/3}Mn_{1/3}O_2$	MCMB	3.8 143	Battery test at 30 ˚C T_d > 390 ˚C	348
Ionogel	Li[TFSA]–[C_3C_1pyrr][TFSA]	Silica	1.9@30 ˚C 4.7@60 ˚C	--	$LiFePO_4$	Li	3.5 155	Battery test at 30–90 ˚C T_d > 195 ˚C	215
Ionogel	Li[TFSA]–[C_2C_1im][TFSA]	Amino-functionalized silica nanofibers	>1.0@25 ˚C	0.22	$LiFePO_4$	Li	3.5 144	Battery test at 65–125 ˚C T_d > 300 ˚C	205
Ionogel	Li[TFSA]–[C_2C_1im][TFSA]	Exfoliated hexagonal boron nitride	>1.0@25 ˚C	0.18	$LiFePO_4$	Li	3.5 160	Battery test at 175 ˚C T_d > 300 ˚C	207
Ionogel	Li[TFSA]–[C_3C_1pyrr][TFSA]	Amine-functionalized boron nitride nanosheets	0.6@25 ˚C	0.23	$LiFePO_4$	Li	3.5 162	Battery test at 80 ˚C T_d > 330 ˚C	98
Ionogel	Li[TFSA]–[C_2C_1im][TFSA]	MOF-525 (Cu)	0.3@25 ˚C 4.9@100 ˚C	0.36	$LiFePO_4$	Li	3.5 145	Battery test at –20–150 ˚C T_d > 300 ˚C Thick positive electrode used (210 μm, 25 mg cm^{-2})	199
Ionogel	Li[TFSA]–[C_2C_1im][TFSA]	TiO_2	2.8@25 ˚C	0.22	$LiFePO_4$	Li	3.5 162	Battery test at room temperature T_d > 370 ˚C	200
Ionogel	Li[TFSA]–[C_4C_1pyrr][TFSA]	TiO_2	1.5@20 ˚C 11.0@80 ˚C	0.15	$LiFePO_4$	Li	3.5 150	Battery test at room temperature T_d > 400 ˚C	206
Ionogel / IPC	Li[FSA]-[N_{1222}][FSA] IPC	PEO	0.2@50 ˚C		$LiFePO_4$	Li	3.5 158	Battery test at 50 ˚C	123
IPC	Na[PF_6]-[$P_{1i4i4i4}$][FSA] IPC		>1@50 ˚C	0.19					142
IPC	Na[FSA]-[$P_{1i4i4i4}$][FSA] IPC		>2@50 ˚C	0.37					142
IPC	Na[TFSA]-[$P_{1i4i4i4}$][FSA] IPC		>2@50 ˚C	0.31					142
IPC	Li[BF_4]-[C_3C_1pyrr][BF_4] IPC		>0.01@25 ˚C						289
IPC	Li[FSA]-[$P_{1i4i4i4}$][FSA] IPC		0.25@22 ˚C		$LiFePO_4$	Li	3.5 160	Battery test at 30 ˚C	124
Ionogel / IPC	Li[FSA]-[C_2C_1pyrr][FSA] IPC	PVDF	5.3×10^{-3}@20 ˚C						335
Ionogel / IPC	Li[TFSA]-[C_2C_1pyrr][FSA] IPC	P(DADMA)-TFSI[b]	0.1@room temp.		$LiFePO_4$	Li	3.5 122 150	Battery test at 25, 40, 80 ˚C	127

IPC	Na[TFSA]-[P_{111i4}][TFSA] IPC		>1@40 ˚C	$NaFePO_4$	Na	163 76	Battery test at 50 ˚C	119
Ionogel / IPC	Li[TFSA]-[C_2C_1pyrr][FSA] IPC	PVDF-HFP	0.3@40 ˚C	$LiFePO_4$	Li	150	Battery test at 30 ˚C	287
Ionogel / IPC	Li[TFSA]-[N_{1222}][FSA] IPC	P(DADMA)-TFSI	0.2@25 ˚C	$LiFePO_4$	Li	150	Battery test at 40 ˚C	306

[a]σ: ionic conductivity by EIS
t_{Li+}: Li^+ transference number by the electrochemical method
T_d: thermal decomposition temperature by TGA

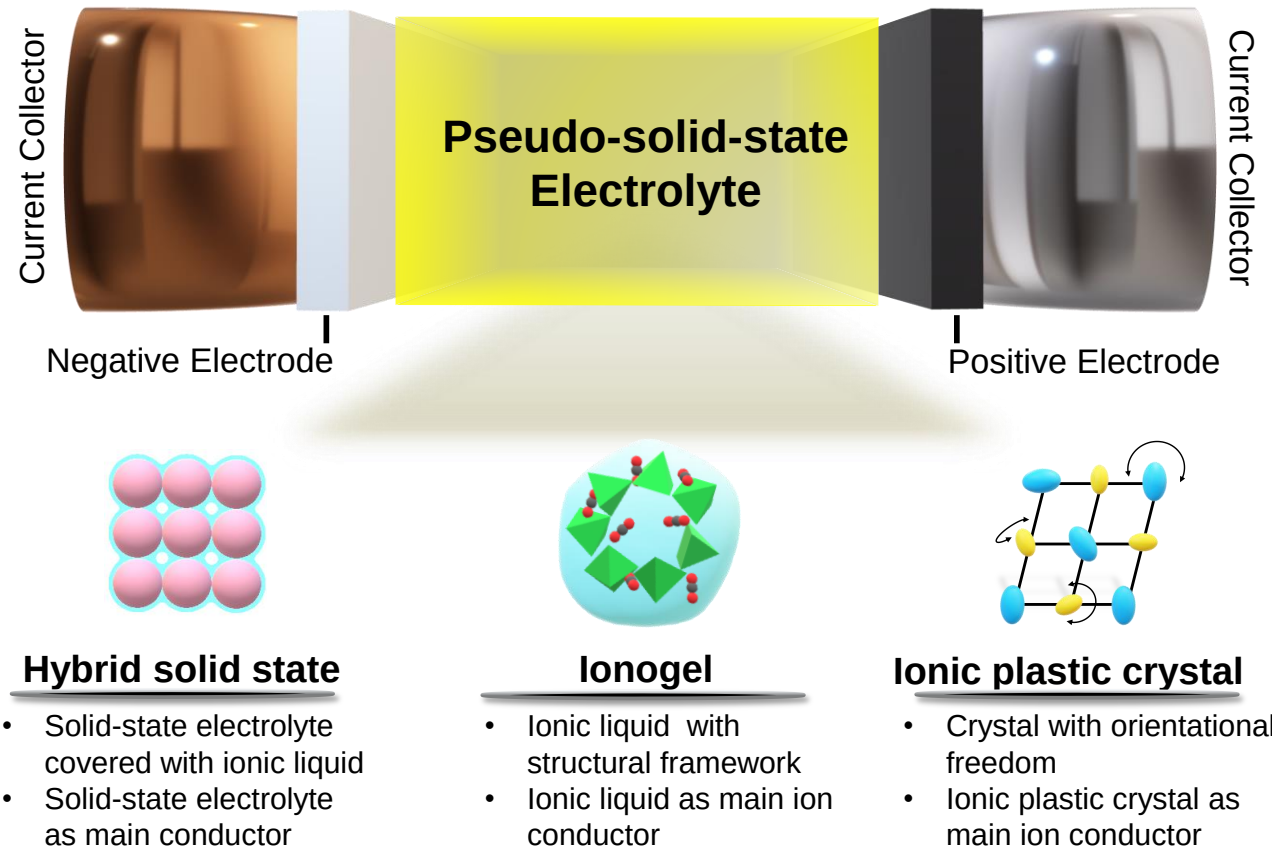

Fig. 1 Schematic illustration of a pseudo-solid-state electrolyte using IL. Hybrid solid-state electrolytes are the composites of a solid-state electrolyte encapsulated in IL. Ionogels are composed of ionically non-conductive host materials coupled with ILs. Ionic plastic crystals typically comprise (pseudo) solid-state electrolytes with disordered ions.

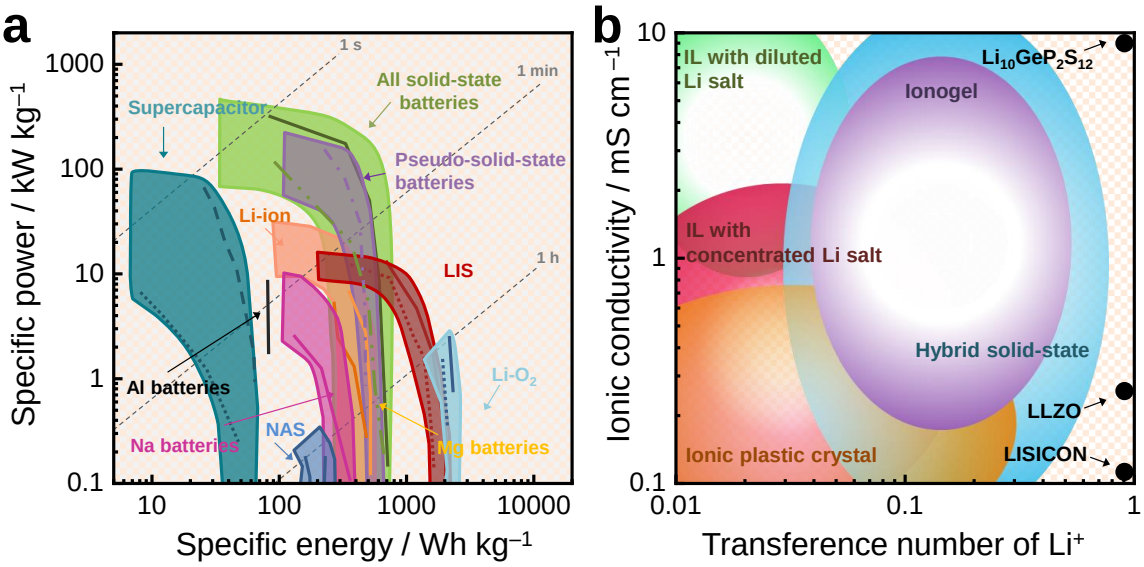

Fig. 2 a. Ragone plot showing the various energy storage systems (i.e. all-solid-state batteries, pseudo-solid-state batteries, NAS, and LIS include data from intermediate temperature operations 50–100 °C), reproduced with the data of previous studies.[5,349] b. Ionic conductivity and transference number of representative electrolytes for Li batteries are arranged based on their properties in Table 1 and the previous studies.[5]

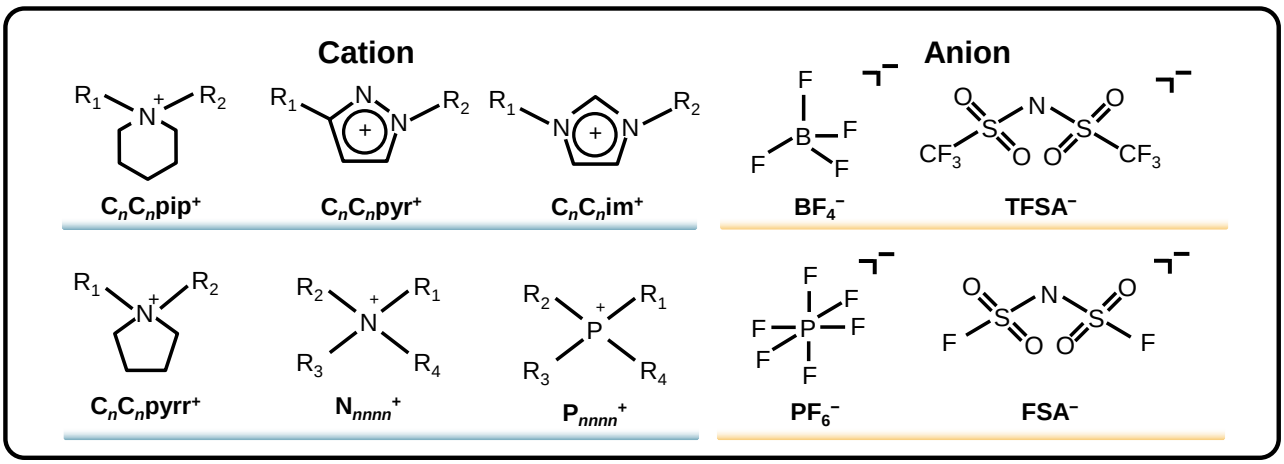

Fig. 3 Representative ionic species in ILs and IPCs for rechargeable batteries. The following abbreviations are used to denote specific ions: $C_nC_npip^+$: *N,N*-dialkylpiperidinium, $C_nC_npyr^+$ = *N,N*-dialkylpyrazolium, $C_nC_npyrr^+$ = *N,N*-dialkylpyrrolidinium, $C_nC_nim^+$ = 1,3-dialkylimidazolium, N_{nnnn}^+ = tetraalkylammonium, P_{nnnn}^+ = tetraalkylphosphonium, BF_4^- = tetrafluoroborate, PF_6^- = hexafluorophosphate, FSA^- = bis(fluorosulfonyl)amide, and $TFSA^-$ = bis(trifluoromethylsulfonyl)amide. The symbol ''*n*'' indicates the number of carbon atoms in the alkyl chain.

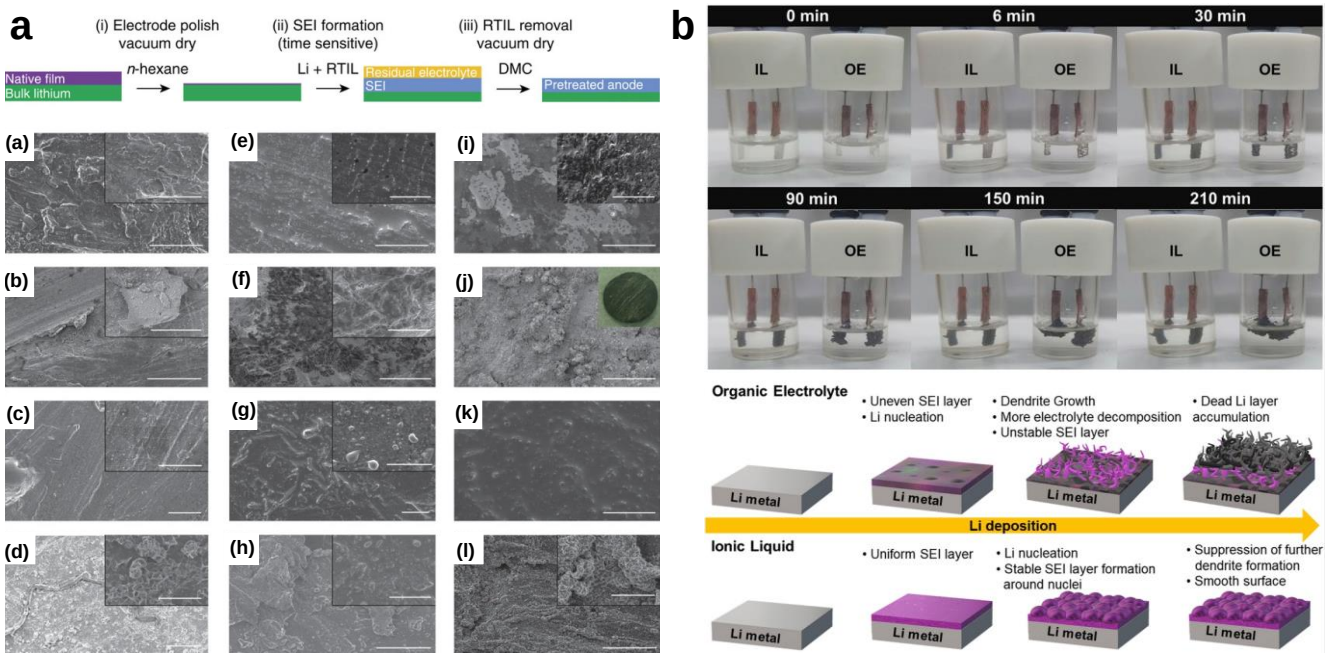

Fig. 4 a. Schematic illustration of Li metal surface treatment using IL and SEM images. (a-d) SEM images of Li metal pre-treated with Li[FSA]-[C_3C_1pyrr][FSA] IL for 4h, 7d, 12d, and 18d, respectively. (e-h) SEM images of Li metal pre-treated with Li[PF_6]-[C_3C_1pyrr][FSA] IL for 4h, 7d, 12d, and 18d, respectively. (i-l) SEM images of Li metal pre-treated with Li[AsF_6]-[C_3C_1pyrr][FSA] IL for 4h, 7d, 12d, and 18d, respectively. b. Images and schematic comparisons of Li deposition and dendrite formation in symmetric Li/Li cells during cycling at 8.0 mA cm^{-2} with organic liquid electrolyte and IL. Reproduced with permission under the Creative Commons Attribution 4.0 International License for a.[183] Reproduced with permission for b.[187] Copyright 2018, Elsevier.

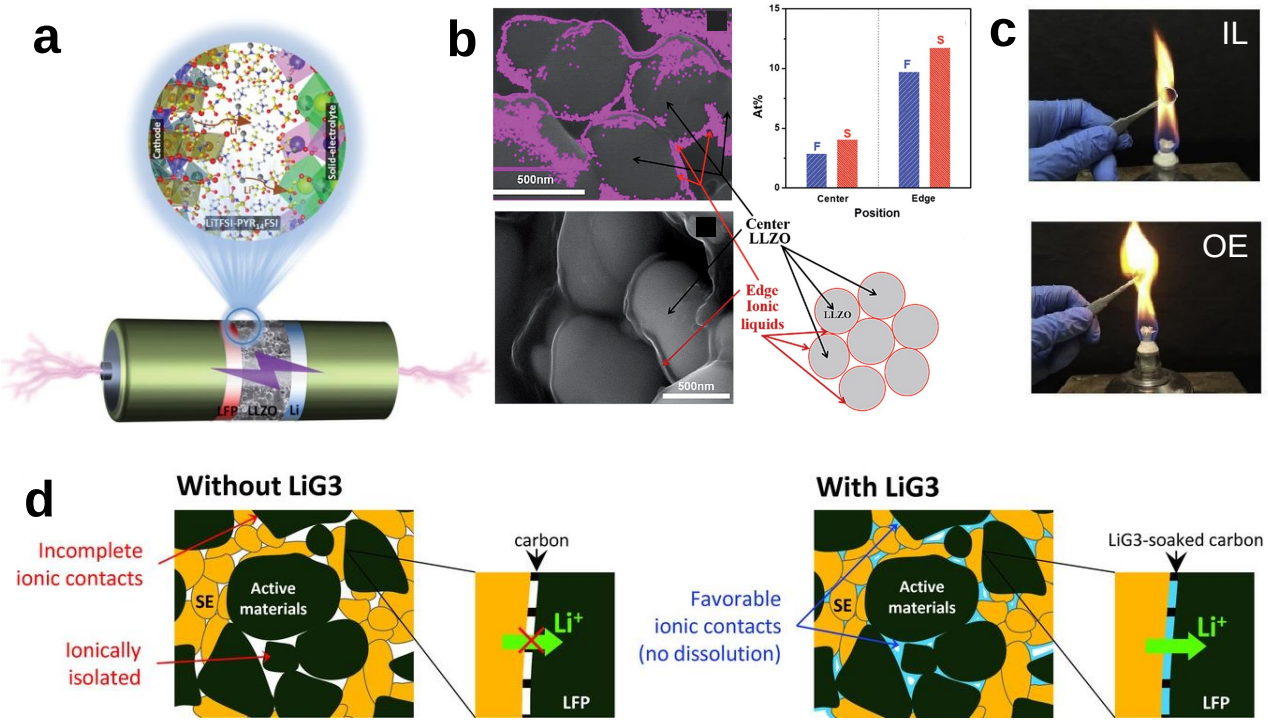

Fig. 5 Interfacial wetting properties for hybrid solid-state electrolytes prepared using ILs. a. Schematic illustration of the interface between LLZO and $LiFePO_4$ electrode. Reproduced with permission.[38] Copyright 2020, Wiley-VCH. b. The FESEM and illustration of LLZO impregnated with IL. Reproduced with permission.[39] Copyright 2016, The Royal Society of Chemistry. c. The optical images of sulfur cathode when approaching the flame after immersion in IL and organic solvent electrolytes. Reproduced with permission.[57] Copyright 2018, Elsevier. d. A schematic diagram representing Li[TFSA]-G3 improves the imperfect solid-solid contacts. Reproduced with permission.[56] Copyright 2015, Wiley-VCH.

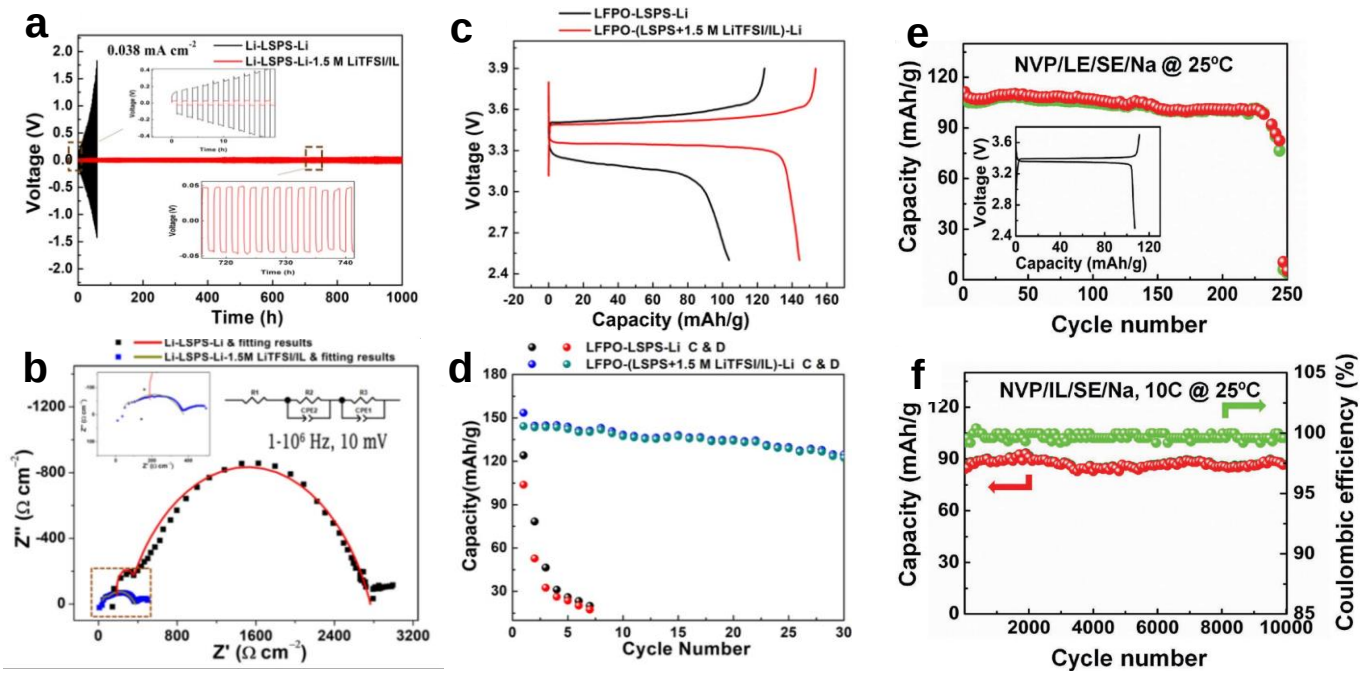

Fig. 6 a. Li deposition-dissolution test employing a Li/$Li_{10}SnP_2S_{12}$/Li symmetric cell with and without the Li[TFSA]-[C_3C_1pyrr][TFSA] IL. b. EIS Nyquist plots of the Li/LSPS/Li symmetric cell with and without the IL. Electrochemical performance of Li/LSPS/$LiFePO_4$ cell with and without IL c. Charge-discharge curves and d. cycle tests Li/LSPS/$LiFePO_4$ cells with and without IL. Reproduced with permission.[55] Copyright 2018, American Chemical Society. Cycle performance of NVP/Na cell e. without IL and f. with IL. Reproduced with permission.[30] Copyright 2017, Wiley-VCH.

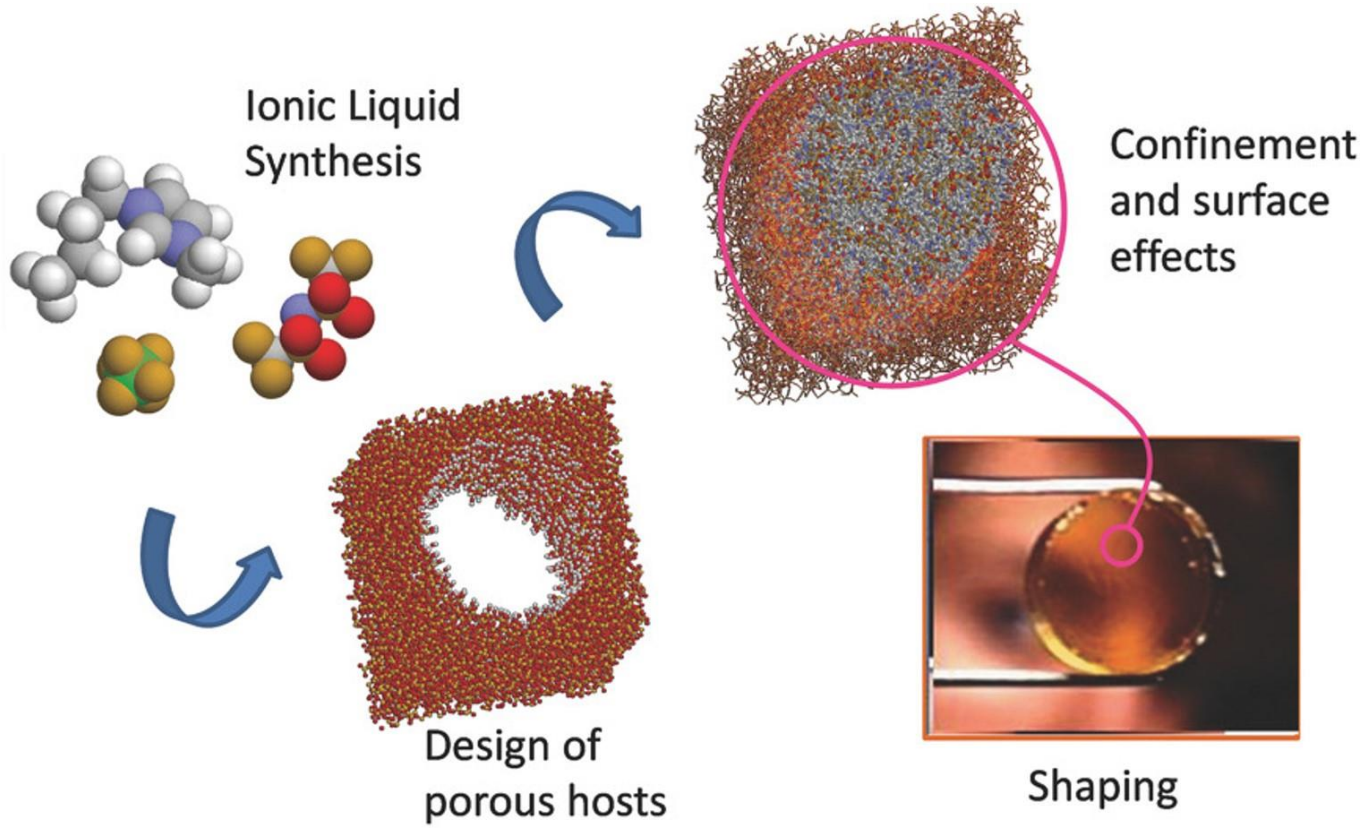

Fig. 7 Schematic diagram showing the casting of ionic liquid in/on a host material to produce ionogels. Reproduced with permission.[189] Copyright 2017, Wiley-VCH

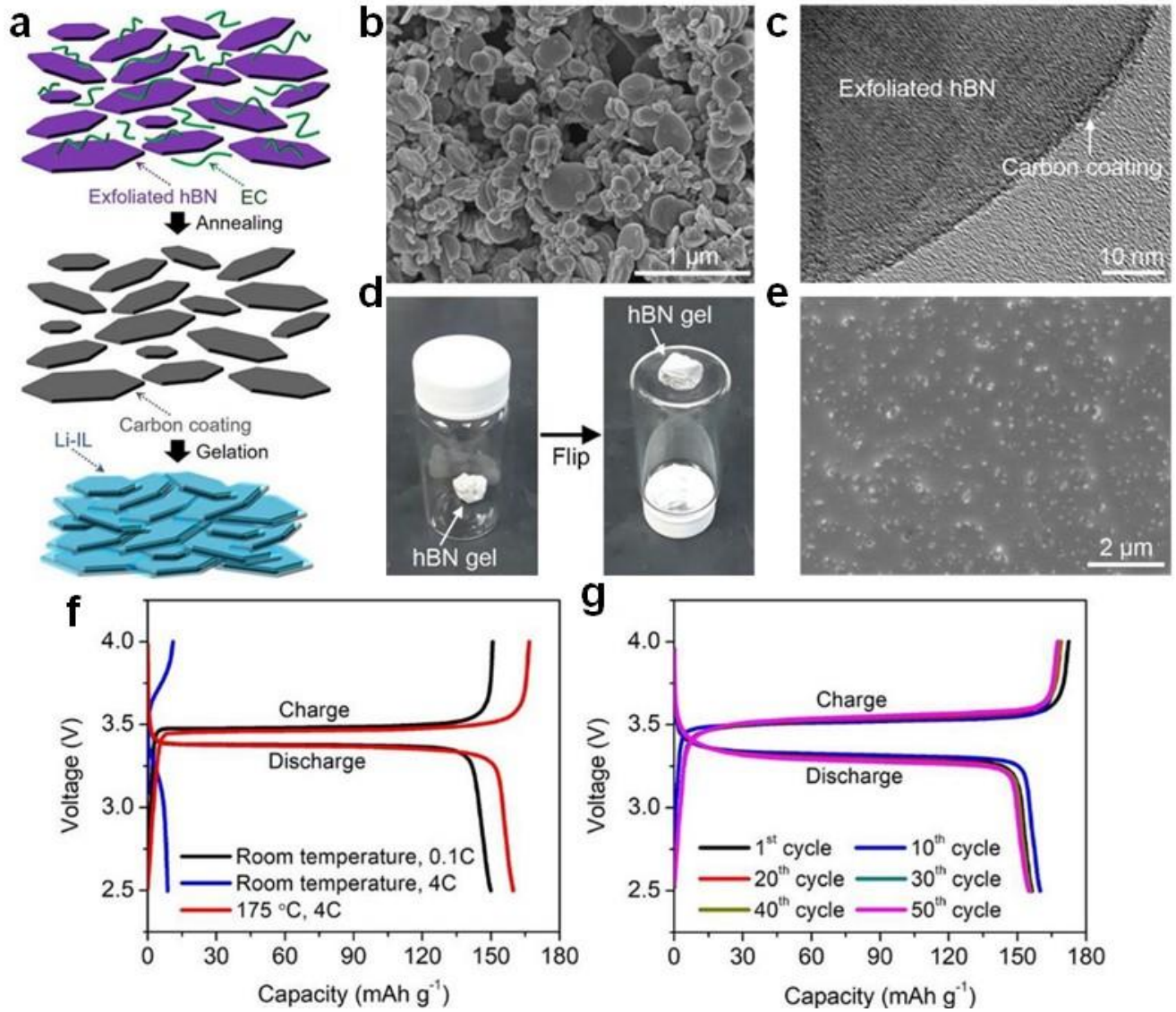

Fig. 8 a. Schematic diagram of hBN gel electrolyte preparation. hBN nanoplatelets are exfoliated from bulk hBN microparticles through liquid-phase exfoliation using ethyl cellulose (EC) stabilisers. The resulting exfoliated hBN/EC powders are annealed at 400 °C for 2 h to decompose the EC, creating a thin carbon coating on the surface of the hBN nanoplatelets. Finally, the hBN nanoplatelets and a Li ionic liquid (Li-IL) are mixed to formulate ionogels. b, c. Scanning and transmission electron microscopy images of the exfoliated, carbon-coated hBN nanoplatelets. d. Photographs of a vial with the hBN ionogels before (left) and after (right) flipping. The electrolyte does not move from the bottom of the inverted vial, confirming the formation of a stable gel. e. SEM images of the hBN gel electrolyte. f. Typical charge-discharge voltage profiles of a Li/hBN/Gr-$LiFePO_4$ cell measured at room temperature and 175 °C, with a voltage window of 2.5–4.0 V. The Gr-$LiFePO_4$ positive electrode is composed of $LiFePO_4$ active materials and graphene conductive additives. g. Charge–discharge voltage profiles of the cell at 10C at 175 °C. Reproduced with permission.[207] Copyright 2019, American Chemical Society.

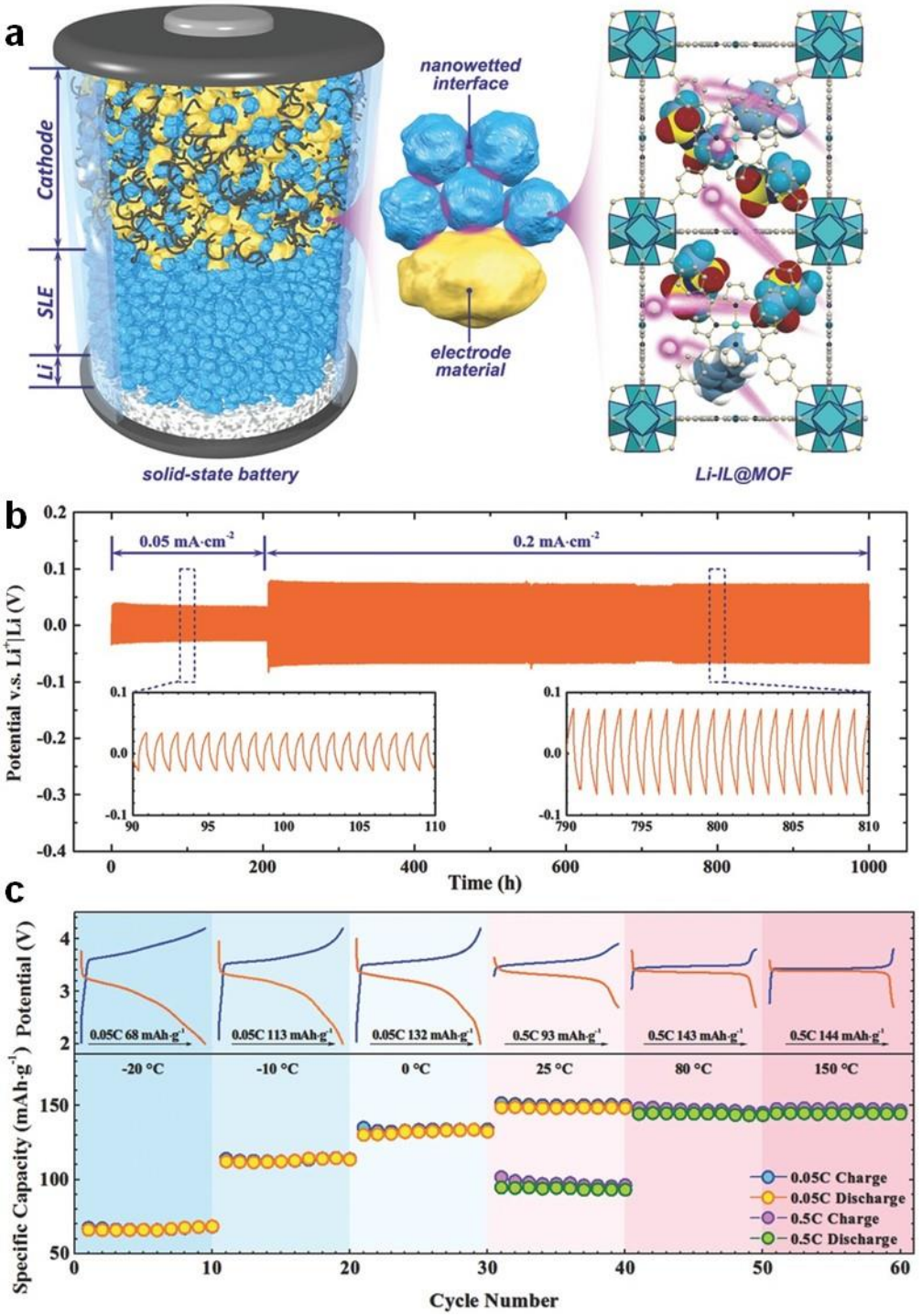

Fig. 9 a. Schematic illustration of the architecture and the nanowetted interfacial mechanism of the solid-state battery with magnification to show crystal structures of the MOF. The $[C_2C_1im]^+$ and $[TFSA]^-$ ions in the space-filling model are randomly displayed in the pores of the MOF. The migrating Li^+ ions are highlighted by glowing pink spheres. Hydrogen atoms are omitted from the MOF structure for clarity. b. Voltage profiles for the Li/Li-IL@MOF/Li symmetric cell at current densities of 0.05 and 0.2 mA cm^{-2}. c. Temperature-dependent cyclability of the Li/Li-IL@MOF/$LiFePO_4$ cell alongside the corresponding charge-discharge curves. Reproduced with permission.[199] Copyright 2018, Wiley-VCH.

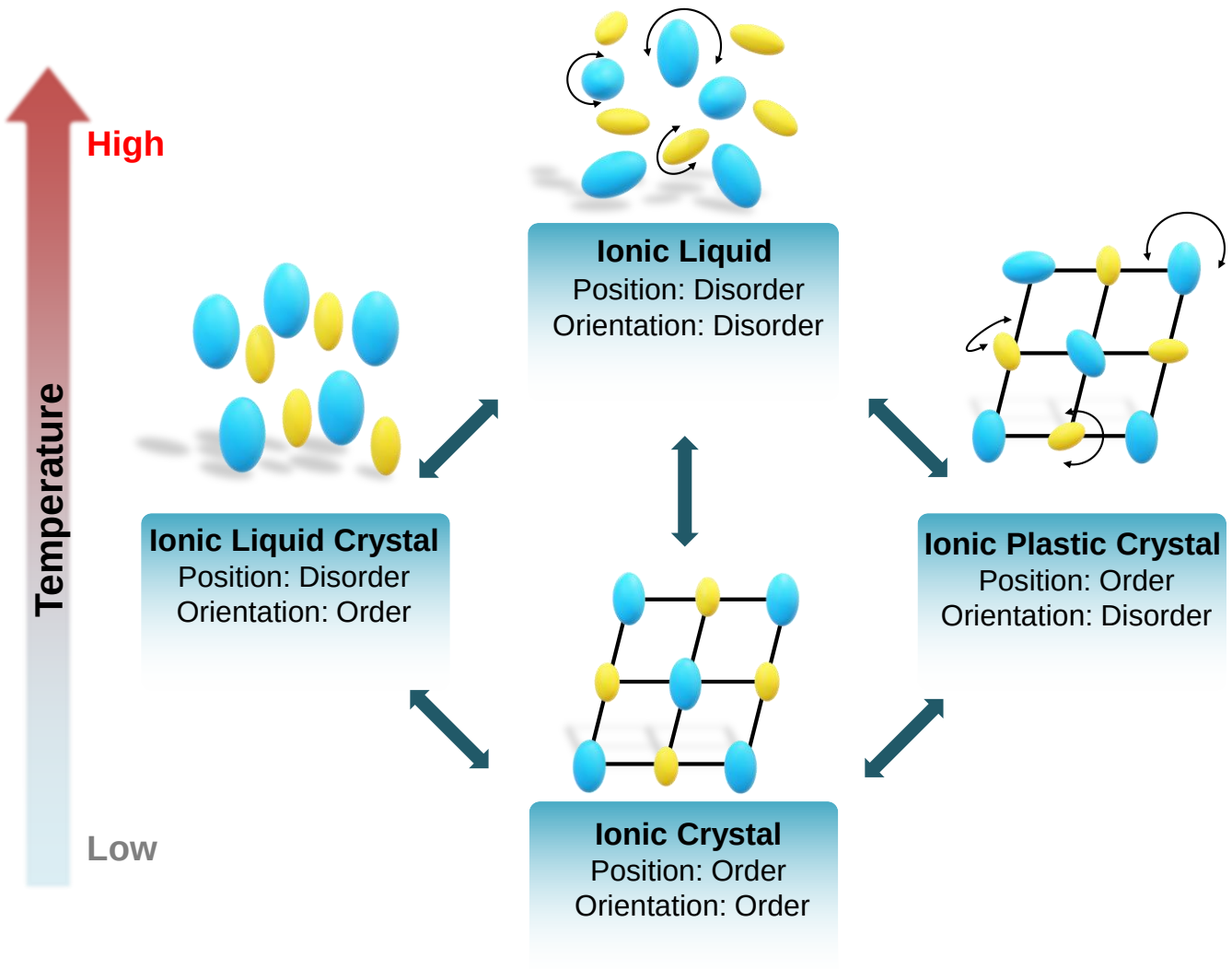

Fig. 10 Schematic showing the structural variation of a salt with an intermediate phase between the crystalline and liquid phase induced by the temperature elevation. In general, IPCs are characterised by orientational disorder and positional order distinct from liquid crystals that have a full or partial positional disorder and orientational order to some degree.

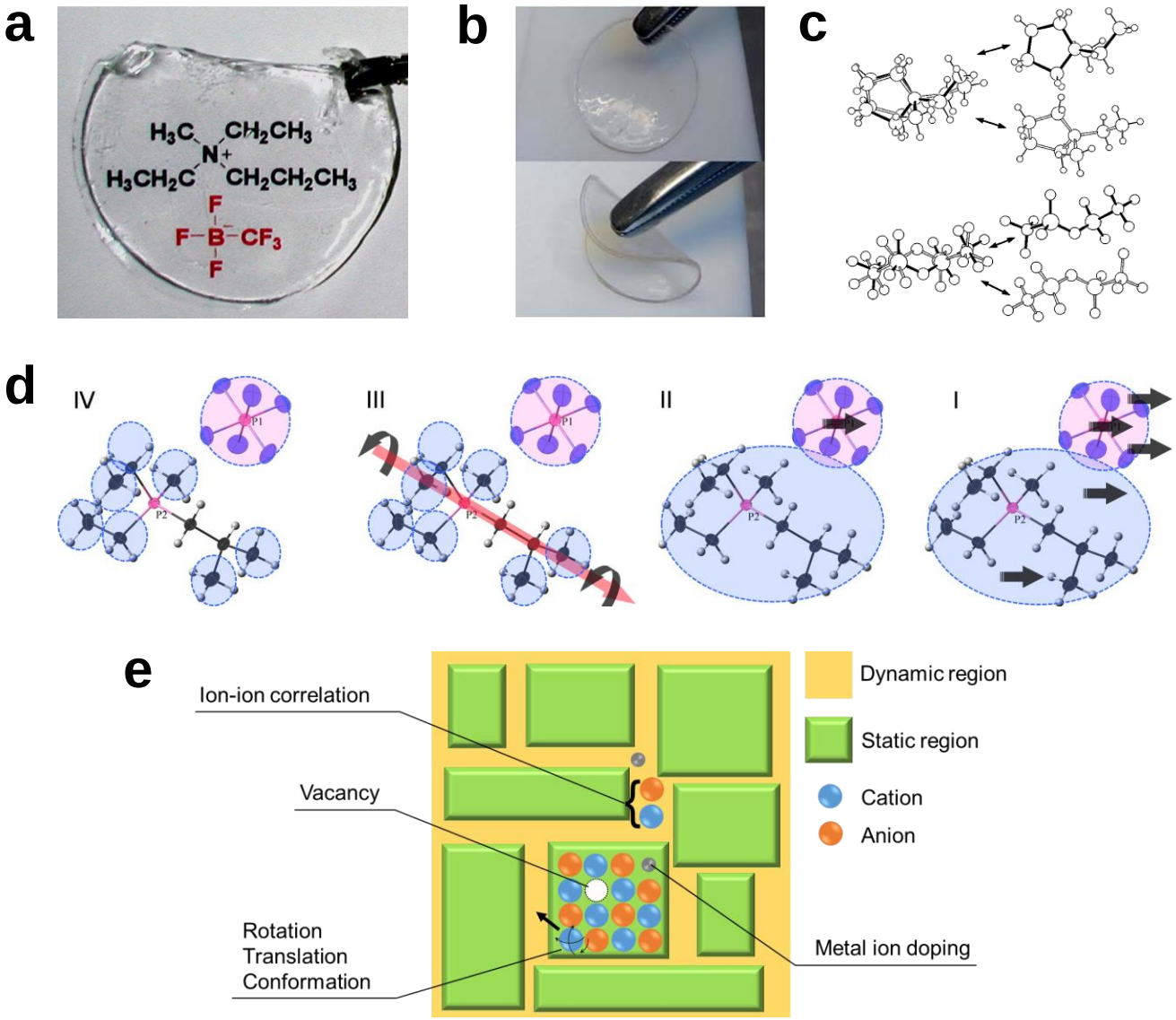

Fig. 11 a. An Image of free-standing IPC film (ca. 50 mm in diameter) of the $[N_{1223}][CF_3BF_3]$ IPC. Reproduced with permission.[255] Copyright 2007, Elsevier. b. Image of the PIL/$[C_2C_1pyrr][FSA]$/Li[TFSA] (PIL: [P(DADMA)][TFSA]) SPE film, reaching a flexion angle of about 180° without breaking. Reproduced with permission.[127] Copyright 2017, The Royal Society of Chemistry. c. Disordering modes of the cation and anion in the $[C_2C_1pyrr][TFSA]$ structure at –60 °C. Reproduced with permission.[258] Copyright 2006, American Chemical Society. d. Schematic of molecular motions in the different phases (IV to I) of $[P_{122i4}][PF_6]$ in response to increasing temperature. Reproduced with permission.[283] Copyright 2012, American Chemical Society. e. Schematic of possible factors affecting ion conduction in IPCs.

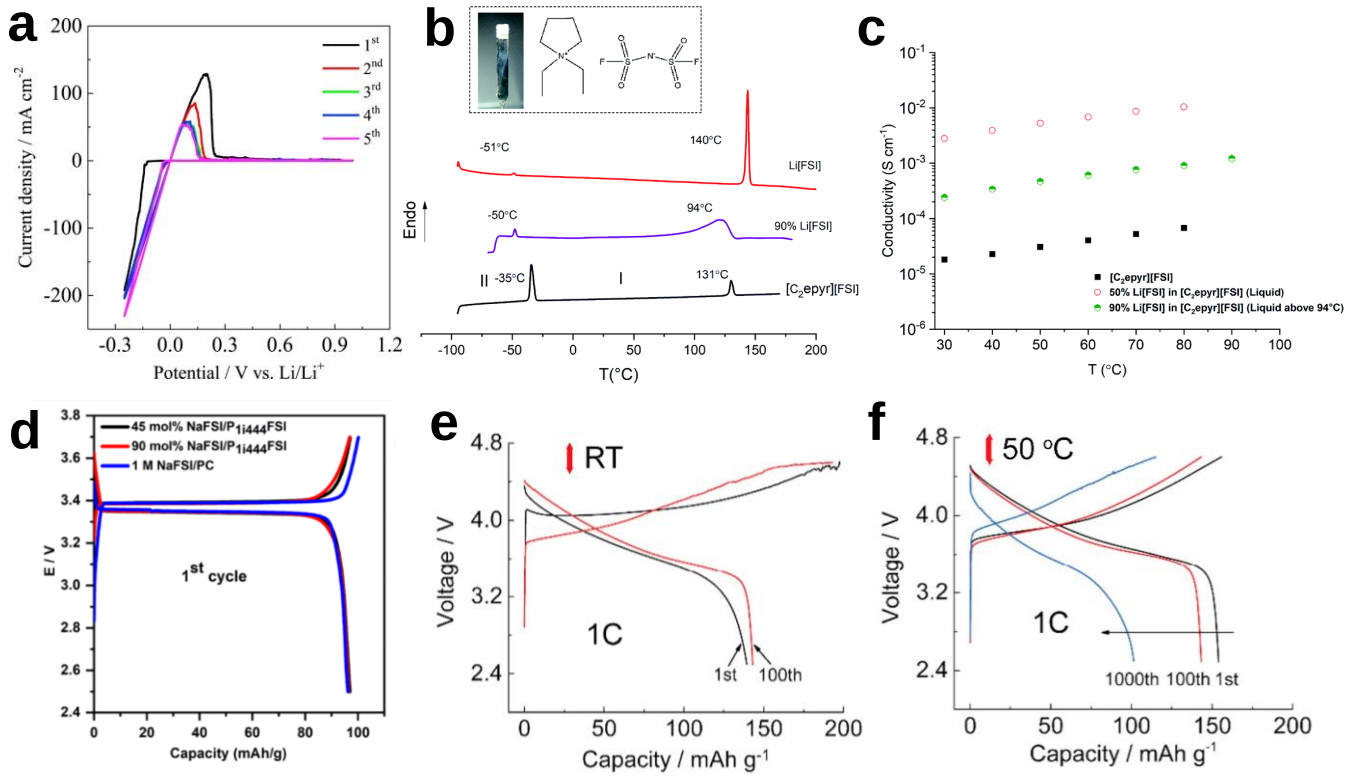

Fig. 12 a. Cyclic voltammograms of a Ni electrode in the 5 mol% Li[FSA]-[C_2C_2pyrr][FSA] IPC at 60 °C, corresponding to Li metal deposition/dissolution. Reproduced with permission.[300] Copyright 2019, Elsevier. b. DSC curves and c. the temperature dependence of ionic conductivity for the 90 mol% Li[FSA]-[C_2C_2pyrr][FSA] quasi-solid state material and those of related materials. The inset of b. indicates the structure of [C_2C_2pyrr][FSA] and a photograph of the quasi-solid state material on a spatula held vertically to demonstrate its solid nature. Reproduced with permission.[321] Copyright 2019, The Royal Society of Chemistry. d. The first cycle charge-discharge curves of the $Na/Na_3V_2(PO_4)_3$ cell with the 90 mol% Na[FSA]-[$P_{1i4i4i4}$][FSA] quasi-solid state material and related electrolytes at 0.2C. Reproduced with permission.[350] Copyright 2020, American Chemical Society. e, f. The charge-discharge curves of the $Li/LiNi_{1/3}Mn_{1/3}Co_{1/3}O_2$ cell with the composite electrolyte of PVDF particles and IPC (60 wt% PVDF-40 wt % IPC (50 mol% Li[FSA]-[C_2C_1pyrr][FSA])) at 1.0C at room temperature (RT) and 50 °C. Reproduced with permission.[338] Copyright 2018, Elsevier.